STABILITY ANALYSIS OF THE CHURCH OF THE NAZARENE VARAX DOME

by

Jacem Tissaoui

Thesis submitted to the Faculty of the
Virginia Polytechnic Institute and State University
in partial fulfillment of the requirements for the degree of
Master of Science
in
Civil Engineering

APPROVED:

Dr. S. M. Holzer, Chairman

Dr. R. H. Plaut

Dr. J. F. Davalos

February 1991

Blacksburg, Virginia

STABILITY ANALYSIS OF THE CHURCH OF THE NAZARENE VARAX DOME

by

Jacem Tissaoui

Committee Chairman: Siegfried M. Holzer
Civil Engineering

(ABSTRACT)

The object of this study is to investigate the stability of the Church of the Nazarene Varax dome under various load distributions. A model of the dome constructed using I-DEAS is presented and results of linear and nonlinear analyses are discussed. A comparison between the critical load obtained using nonlinear analysis and combined linear and nonlinear analysis is made. The model is modified to include flexible joints and bracing to model the decking. The effect of these modifications on the critical load is discussed.

ACKNOWLEDGEMENTS

The author wishes to express his gratitude to Dr. S. M. Holzer for his support and advice throughout this study. He also would like to thank Dr. Raymond H. Plaut and Dr. Julio F. Davalos for serving on his committee and for providing helpful suggestions. He also wishes to thank Donald L. Broyles for introducing him to I-DEAS and Chiung-Yu Huang for his assistance with ABAQUS. Finally the author would like to thank his family for their support throughout the years.

TABLE OF CONTENTS

1. INTRODUCTION 1

2. THE VARAX DOME MODEL 3

2.1 INTRODUCTION 3

2.2 GEOMETRY OF THE DOME 3

2.3 I-DEAS 4

2.3.1 The Engineering Analysis family 5

2.3.2 Preprocessing 5

2.4 ABAQUS 6

2.5 CONSTRUCTION OF THE MODEL 6

2.6 THE B33 BEAM ELEMENT 17

2.7 MATERIAL MODELING 17

2.8 BOUNDARY CONDITIONS 18

2.9 LOADS 21

2.9.1 Design Loads 21

2.9.2 Load Discretization 21

3. LINEAR ANALYSIS OF THE DOME 25

3.1 PURPOSE 25

3.2 PROCEDURE 25

3.3 RESULTS 26

3.3.1 Uniform snow load 26

3.3.2 Inner snow load 27

3.3.3 Outer snow load 27

3.3.4 Snow over half the dome 27
4. NONLINEAR ANALYSIS OF THE DOME 36
4.1 PURPOSE 36
4.2 NONLINEAR ANALYSIS METHODS 36
4.3 PROCEDURE 37
4.4 RESULTS 38
4.4.1 Uniform snow load 38
4.4.2 Inner snow load 43
4.4.3 Outer snow load 49
4.4.4 Snow over half the dome 53
5. COMBINED LINEAR AND NONLINEAR ANALYSIS 57
5.1 OVERVIEW 57
5.2 PROCEDURE 57
5.3 RESULTS OF THE ANALYSES 60
5.3.1 Uniform snow load 62
5.3.2 Inner snow load 64
5.3.3 Outer snow load 66
5.3.4 Snow over half the dome 68
6. FLEXIBLE JOINTS 70
6.1 INTRODUCTION 70
6.2 THE VARAX JOINTS 70
6.3 ALTERNATIVES FOR MODELING THE JOINTS 72
6.4 STIFFNESS REDUCTION FACTOR 73
6.5 MODELING THE JOINTS USING I-DEAS 75
6.6 MODIFICATIONS TO THE DOME MODEL 75

6.7 RESULTS OF THE ANALYSES 77
7. MODELING OF THE EFFECT OF THE DECKING 80
7.1 OVERVIEW 80
7.2 MODELING OF THE DECKING 80
7.3 PROCEDURE 84
7.4 RESULTS 84
7.4.1 Uniform snow load 84
7.4.2 Snow over half the dome 84
7.5 DISCUSSION OF THE RESULTS 87
8. CONCLUSIONS AND RECOMMENDATIONS 88
8.1 CONCLUSIONS 88
8.2 RECOMMENDATIONS 89
REFERENCES 90
APPENDIX A 91
VITA 94

LIST OF ILLUSTRATIONS

Figure 2.1: Nodes of one sector as seen in plan view 8

Figure 2.2: Main beams for one sector 10

Figure 2.3: Beams, purlins and steel ring for one sector 11

Figure 2.4: Triangular shell elements of one sector 11

Figure 2.5: Shell elements for entire dome 13

Figure 2.6: Beams, purlins and steel ring for entire dome 14

Figure 2.7: Boundary conditions shown at the 14 perimeter nodes 19

Figure 2.8: Close-up view of a node where boundary conditions are applied 20

Figure 2.9: Inner snow load 23

Figure 2.10: Outer snow load 23

Figure 2.11: Snow over half the dome 24

Figure 3.1: Displacement contours for uniform snow load 29

Figure 3.2: Maximum combined axial and bending stresses for uniform snow 30

Figure 3.3: Displacement contours for inner snow load 31

Figure 3.4: Maximum combined axial and bending stresses for inner snow load 32

Figure 3.5: Displacement contours for outer snow load 33

Figure 3.6: Maximum combined axial and bending stresses for outer snow load 34

Figure 3.7: Displacement contours for snow over half the dome 35

Figure 4.1: Equilibrium paths at nodes 1, 3, 5, and 8 for uniform snow load 40

Figure 4.2: Buckling mode for uniform snow load 41

Figure 4.3: Maximum stresses in beams just before buckling 42

Figure 4.4: Buckled shape for inner snow load 44

Figure 4.5: Equilibrium paths at the apex (3), steel ring (1) and node 70 45

Figure 4.6: Equilibrium paths for lateral displacements at node 70 46
Figure 4.7: Equilibrium paths for nodes 148 and 149 47
Figure 4.8: Maximum stresses just before buckling for inner snow load 48
Figure 4.9: Buckling mode for outer snow load 50
Figure 4.10: Equilibrium paths at the apex (3) and steel ring (1) for outer snow load 51
Figure 4.11: Maximum stresses just before buckling for outer snow load 52
Figure 4.12: Buckling mode for snow over half the dome 54
Figure 4.13: Equilibrium paths at nodes 67 and 149 55
Figure 4.14: Equilibrium paths for nodes 1, 3, 5 and 8 56
Figure 5.1: Critical load parameters 61
Figure 5.2: Critical load prediction for uniform snow load 63
Figure 5.3: Critical load prediction for inner snow load 65
Figure 5.4: Critical load prediction for outer snow load 67
Figure 5.5: Critical load prediction for snow over half the dome 69
Figure 6.1: The Varax joint 71
Figure 6.2: Modeling of the beam connections (at apex) 72
Figure 6.3 (a) original beam dimensions 74
(b) connector beam element with reduced dimensions 74
Figure 6.4: Shell element mesh for flexible joint model 76
Figure 7.1: Bracing for entire dome 82
Figure 7.2: Bracing on entire dome (a) cross bracing; (b) longitudinal bracing 83
Figure 7.3: Buckled shape for uniform snow load 85
Figure 7.4: Buckled shape for snow over half the dome 86

LIST OF TABLES

Table 5.1: Buckling load prediction for uniform snow load.....62

Table 5.2: Buckling load prediction for inner snow load.....64

Table 5.3: Buckling load prediction for outer snow load.....66

Table 5.4: Buckling load prediction for snow over half the dome.....68

Table 6.1: Connector element dimensions for 3 stiffness reduction factors.....74

Table 6.2: Critical load factors for uniform snow load.....78

Table 6.3: Critical load factors for inner snow load.....78

Table 6.4: Critical load factors for outer snow load.....79

Table 6.5: Critical load factors for snow over half the dome.....79

1. INTRODUCTION

The purpose of this study is to investigate the stability of the Church of the Nazarene Varax dome (Covalis, Oregon) under various load distributions. The dome model is built using I-DEAS and analyzed using ABAQUS. I-DEAS was used because of its graphical capabilities which allow for fast and efficient construction of complicated models. It is also used to get a graphical interpretation of the results. ABAQUS is used because of its nonlinear analysis capabilities and because it is simple to use.

First, linear analysis is conducted gain an insight of the behavior of the dome that could help in nonlinear analysis and to verify the model. Then nonlinear analyses are conducted for uniform snow load, inner snow load, outer snow load, and snow over half the dome to determine the critical snow load. To get a more realistic model of the dome, flexible joints and bracing are introduced and their effects on the critical load are assessed.

Two methods are used to obtain the critical snow load. The first method is nonlinear analysis where the equilibrium path is traced up to a critical point, and the second method is a combined linear and nonlinear analysis where we solve an eigenvalue problem to get the critical snow load. The two methods

are compared to determine if the combined linear and nonlinear analysis can be used to predict critical loads accurately.

2. THE VARAX DOME MODEL

2.1 INTRODUCTION

In past research the dome model was constructed using fortran programs to write input files for ABAQUS. These fortran programs define the nodal coordinates and element connectivities. This method was efficient for a particular class of domes; however, it is not flexible because it is difficult to check the model or to make modifications, especially when dealing with complex structures. The method used in this research combines the powerful numerical abilities of ABAQUS with the convenient and friendly pre and postprocessing capabilities of I-DEAS.

2.2 GEOMETRY OF THE DOME

Most of the information on the Church of the Nazarene dome was obtained through a private communication from R. Eshelby, the design engineer in charge.

The Church of the Nazarene dome has a span of 130.6 ft, a rise of 22.4 ft and a radius curvature of 106.5 ft. The dome consists of seven identical sectors and is supported by fourteen columns (two columns at each sector). The dome is also supported at the perimeter by a steel tension ring with a 5 in^2 cross sectional area. The dome consists of 77 beams and 112 purlins. The beams and purlins lie in great circle planes defined by the intersection of a plane passing through the center of the sphere and the the surface of the sphere. The beams are interconnected by patented Varax connectors. The dome is covered with 2-in. tongue-and-groove wood decking.

2.3 I-DEAS

I-DEAS, which stands for Integrated Design Engineering Analysis System, is an integrated package of software tools which is intended to help in the analysis and design in different fields [8]. I-DEAS consists of a number of families which are further divided into modules. All the families share the same database and are executed from the same menu. The I-DEAS families are:

- **Solid Modeling:** Contains object modeling and system assembly.

- **Engineering Analysis:** Converts geometry into a finite element model used to analyze the effects of structural and thermal loads.

- **System Dynamics:** Used for finite element vibration analyses.

- **Test Data Analysis:** Allows the graphic representation of the numerical results in 2D or 3D.

- **Drafting.**

2.3.1 The Engineering Analysis family

All of the modeling and pre and postprocessing for this research was conducted in the Engineering Analysis family. The family's main modules are Pre-processing where the model is created, Model Solution where the finite element analysis is conducted and Postprocessing where the results of the analysis can be graphically displayed using deformed geometry and contour plots.

2.3.2 Preprocessing

This module allows the creation of a model of the structure. It is divided into tasks; the main tasks are:

- **Model Preparation:** This task is used to define the nodes, the elements, and their material and physical properties.

• **Model Checking:** After the model creation, the model checking task can be used to detect coincident nodes or elements, or incorrect node or element locations.

• **Analysis Cases:** This task is used to apply boundary conditions and structural or thermal loads. Combinations of loads and boundary conditions are stored in different case sets where each case set consists of a load case and a restraint case.

• **Pearl Database:** This database allows the transfer of data between families. It is also used to write input files for different finite element analysis programs.

• **Data Loaders:** This task converts output files from finite element analyses into universal files which can be read by I-DEAS for postprocessing.

2.4 ABAQUS

ABAQUS is a general-purpose finite element system intended for a variety of applications. It is well known for its nonlinear capabilities which include automatic incrementation.

2.5 CONSTRUCTION OF THE MODEL

The model was constructed in 6 steps:

1- Define the nodes for one sector:

The node coordinates for the dome were included in Eshelby's report [10]; however, since the model he used did not include purlins, nodes had to be generated between the nodes of every main beam so that the purlins could be defined. The BEtween_nodes command was used to generate equally spaced nodes between existing nodes. Figure 2.1 shows the nodes in one sector.

In I-DEAS, nodes are created in the model preparation task. The Create command lets the user enter the coordinates of the nodes in the specified coordinate system. Once the nodes are created, they can be seen on the screen using the AU (AUtoscale) command.

The command sequence for creating the nodes is:

- Select **node** from the main menu in the Model Preparation Task.
- Select **create** from the node menu.
- Respond to the prompts.
- Enter **done** when finished, or press return.

To create nodes in between two nodes:

- Select **between** from the node menu.
- Select the first node.
- Select the second node.
- Enter the number of nodes in between.
- Select the appropriate coordinate system.

- Confirm the node creation.

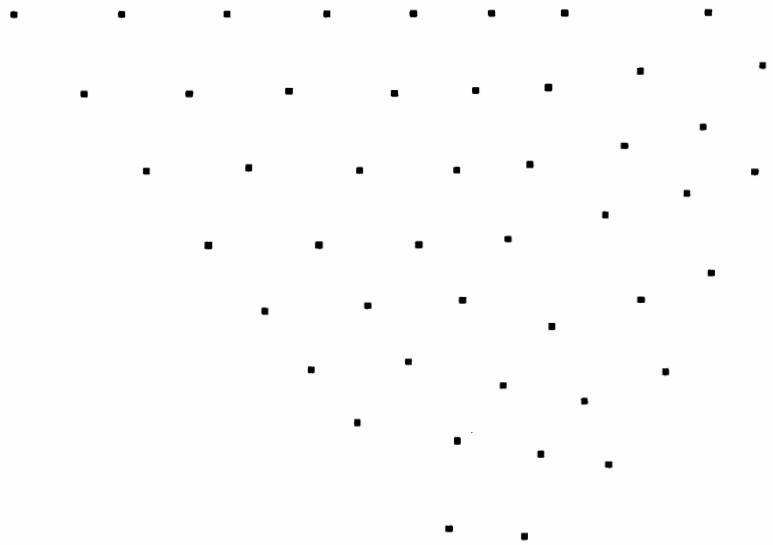

Fig. 2.1: Nodes of one sector as seen in plan view.

2- Define all the elements for the sector:

The elements are also defined in the model preparation task. There are many options for creating elements; the one used here is single element creation. This allows the user to create the elements one by one by selecting the nodes that define it. Before the elements are created, the user is asked to enter the physical and material properties of the elements or to accept the default values; in this case the default values were accepted since the properties will be defined using a fortran program. Figures 2.2, 2.3, and 2.4 show the elements in one sector.

The elements created were:

- Main beams
- Purlins
- Edge beams
- Steel ring
- Shell elements

The commands used to create single elements are:

- Select **element** from the Model Preparation menu.
- Select **default**.
- Set the default element type and color.
- Select **create** from the element menu.
- Accept the default element type or select the appropriate one.
- Accept the default physical property table or create a new one.
- Accept the default material property table or create a new one.
- Select the connecting nodes.

- Select **done** when finished.

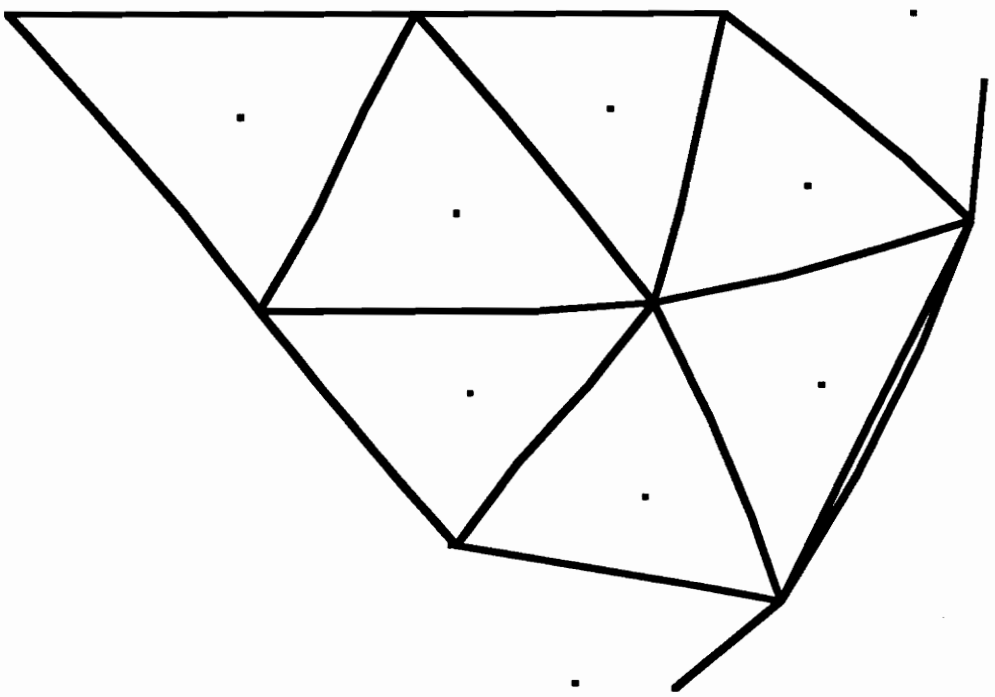

Fig. 2.2: Main beams for one sector.

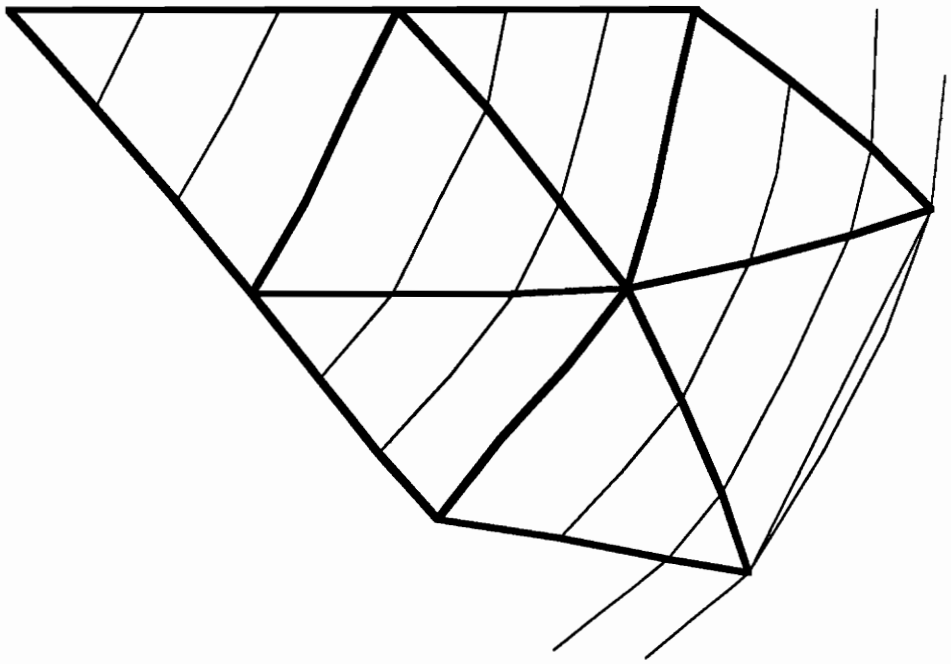

Fig. 2.3: Beams, purlins and steel ring for one sector.

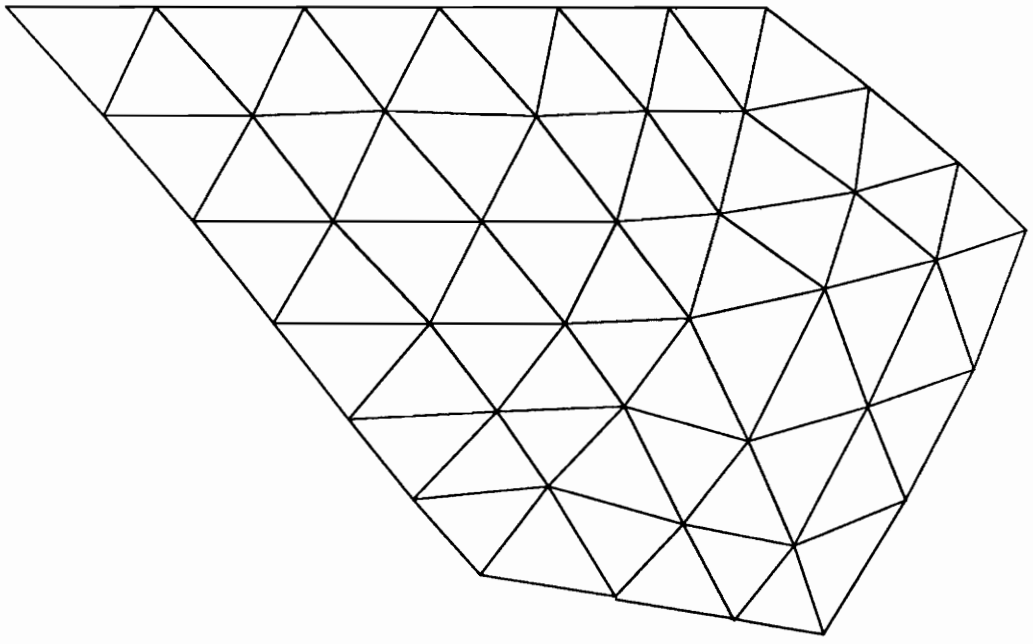

Fig. 2.4: Triangular shell elements of one sector.

3- Reflect the sector to obtain the complete dome:

Once one sector is defined, it is reflected about an axis passing through the center of the dome and two nodes on the edge of that sector using the reflect command. An identical sector that defines the second sector of the dome is then created. This procedure is repeated until all seven sectors are created. Figures 2.5 and 2.6 show the elements for the entire dome.

The following commands are used to reflect elements:

- Select create from the element menu.
- Select reflect.
- Select the method of reflection (the 3 point method is used here).
- Select three points that define the plane about which the sector will be reflected.
- Respond to the prompts.
- Confirm element creation.

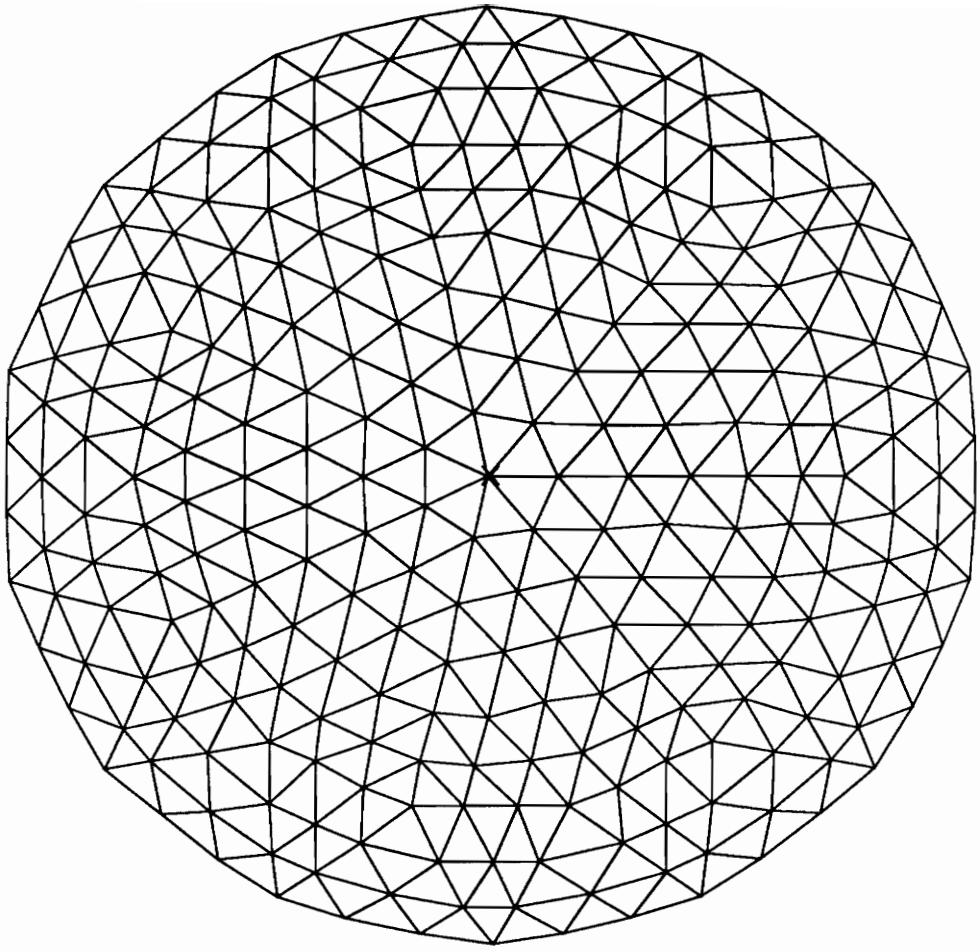

Fig. 2.5: Shell elements for entire dome.

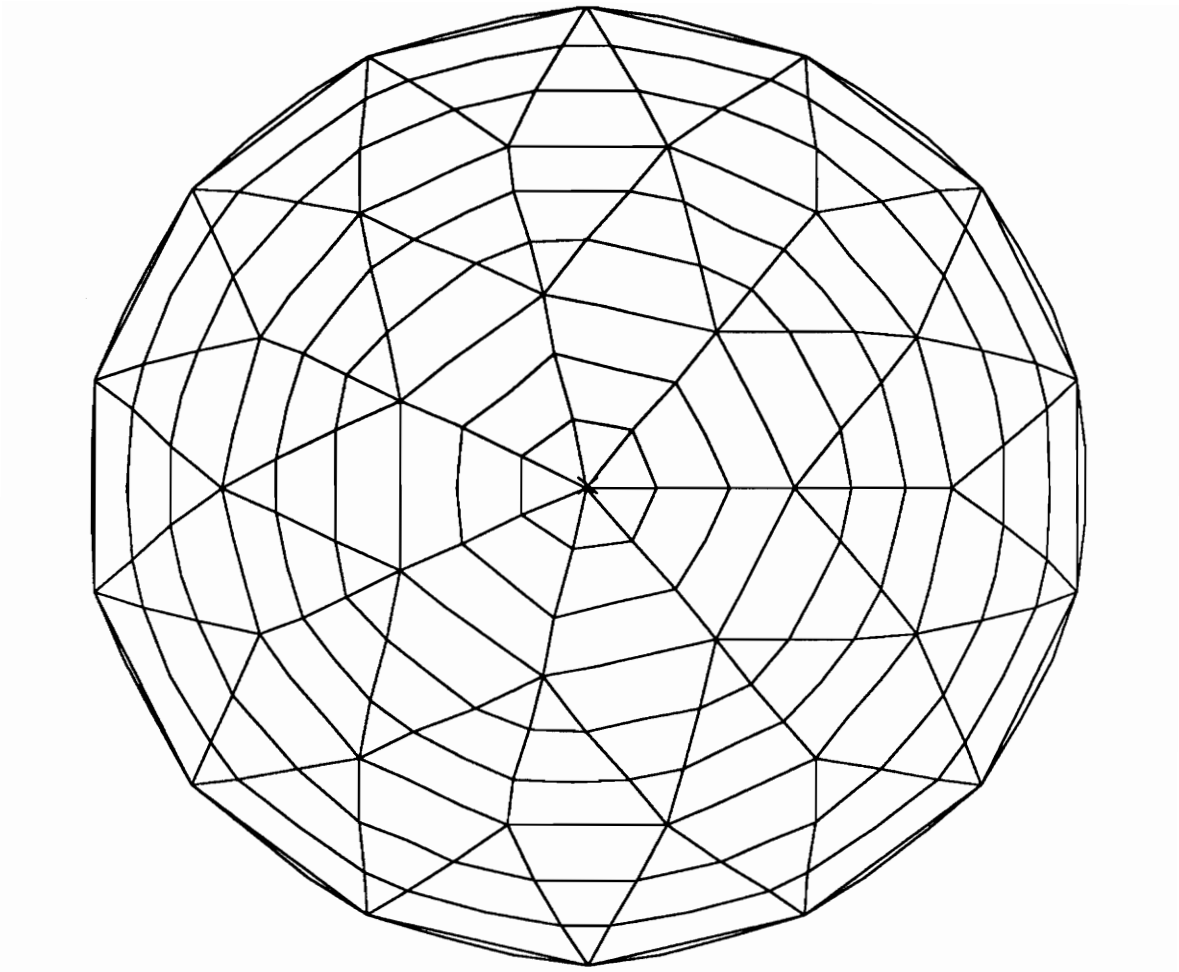

Fig. 2.6: Beams, purlins and steel ring for entire dome.

4- Check the model:

As the model is constructed, it is easy to visually detect any flaws in the geometry of the model. Also, the model can be checked for node and element coincidence using the MODEL_CHECKING task. Nodes are checked for coincidence within a specified range; the coincident nodes are shown on the screen and the user can then merge them. Once the coincident nodes are

merged, the extra nodes have to be deleted; an efficient way of deleting them is to delete all the nodes, which will only delete the extra nodes since nodes connected to elements will not be deleted.

Another useful check is the one for element coincidence. Two elements are considered to be coincident if they have the same nodes.

To check for node coincidence:

- Choose the Model Checking task.
- Select **node coincidence.**
- Select the nodes to be checked (usually all the nodes).
- Enter the range within which nodes are considered to be coincident.
- Confirm merging the coincident nodes.
- Delete the coincident nodes.

To check for coincident elements:

- Select **element coincidence.**
- Select the elements to be checked (usually all the elements).
- Delete the coincident elements.

5- Write the input file for ABAQUS:

There are two steps involved in writing the input file for ABAQUS:

- **Open a Pearle database file and load the model.**

1- Choose the PEARL task

2- Open a new database (Open)

3- Load the model (Load MOdel)

4- Save the database (CLOse)

- **Use the Manage_File task to write the ABAQUS input file.**

1- Choose WRITE from the menu.

2- Choose ab for ABAQUS

3- Input the information requested:

- Name of the Pearl Database file.
- Name of the ABAQUS input file.

When finished, the user gets a message stating whether or not the opearion was successful.

6- Use a Fortran program to define the section properties of the beams.

Because most elements in the model have different direction cosines, it was not possible to generate the physical property data for the elements with I-DEAS.

A fortran program was written (Appendix A) to calculate the direction cosines of the beams and purlins, and to write the physical property cards for each element.

7- Edit the input file to include step definitions and loads.

Once the model is defined, step definition cards and boundary condition cards are added to the input file.

2.6 THE B33 BEAM ELEMENT

B33 elements were used to model the beams and purlins. The B33 beam element [1] is a two-node cubic interpolation beam based on the Euler-Bernoulli beam theory, which ignores transverse shear deformations. This assumption is valid since the beam elements have a large aspect ratio. Also, results obtained from linear analysis for a Varax dome model with B32 beam elements (three-node parabolic beam based on the Timoshenko beam theory which accounts for shear deformations) yielded results very close to the ones from the model with the B33 beam elements.

2.7 MATERIAL MODELING

The beams and purlins in the Varax dome are made of glued-laminated southern pine timber. To simplify the analysis, the material is considered to be transvesly isotropic, this assumption is verified in [4]. The Young modulus is 1,800,000 psi and the shear modulus is 160,000 psi. However, since the the beam model used does not account for shear deformations, the shear modulus is not included in the material property information.

2.8 BOUNDARY CONDITIONS

The boundary conditions have to satisfy the following conditions:

- Rigid body motion should not be allowed to avoid singularities.
- The boundary conditions should allow the tension ring to move radially.

As an alterative to the approach used by Davalos in [3], where restraints are applied at the apex and at four radially opposed nodes on the steel ring (fig. 2.7), the boundary conditions are applied at the fourteen steel ring nodes where the supporting columns are connected. First the restrained nodes are assigned cylindrical displacement coordinates using the TRANSFORM card in ABAQUS. This defines the displacement coordinates as translations and rotations in the radial, tangential and vertical directions. Then, the nodes are restrained from translating in the vertical and tangential directions while allowed to translate in the radial direction and to rotate in any direction.

No constraints are applied at the interior nodes which does not account for the stiffening effect of the decking. The arrows in figs. 2.7 and 2.8 show the directions where restraints are applied.

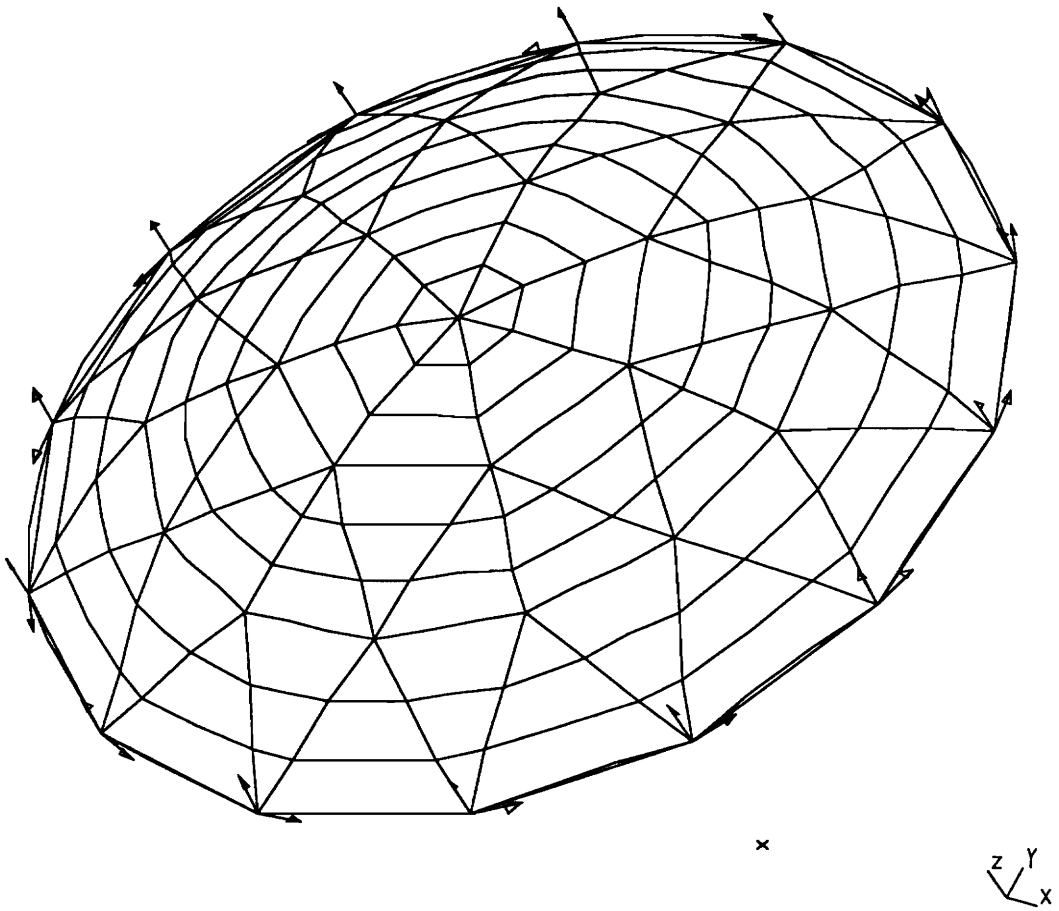

Fig. 2.7: Boundary conditions shown at the 14 perimeter nodes

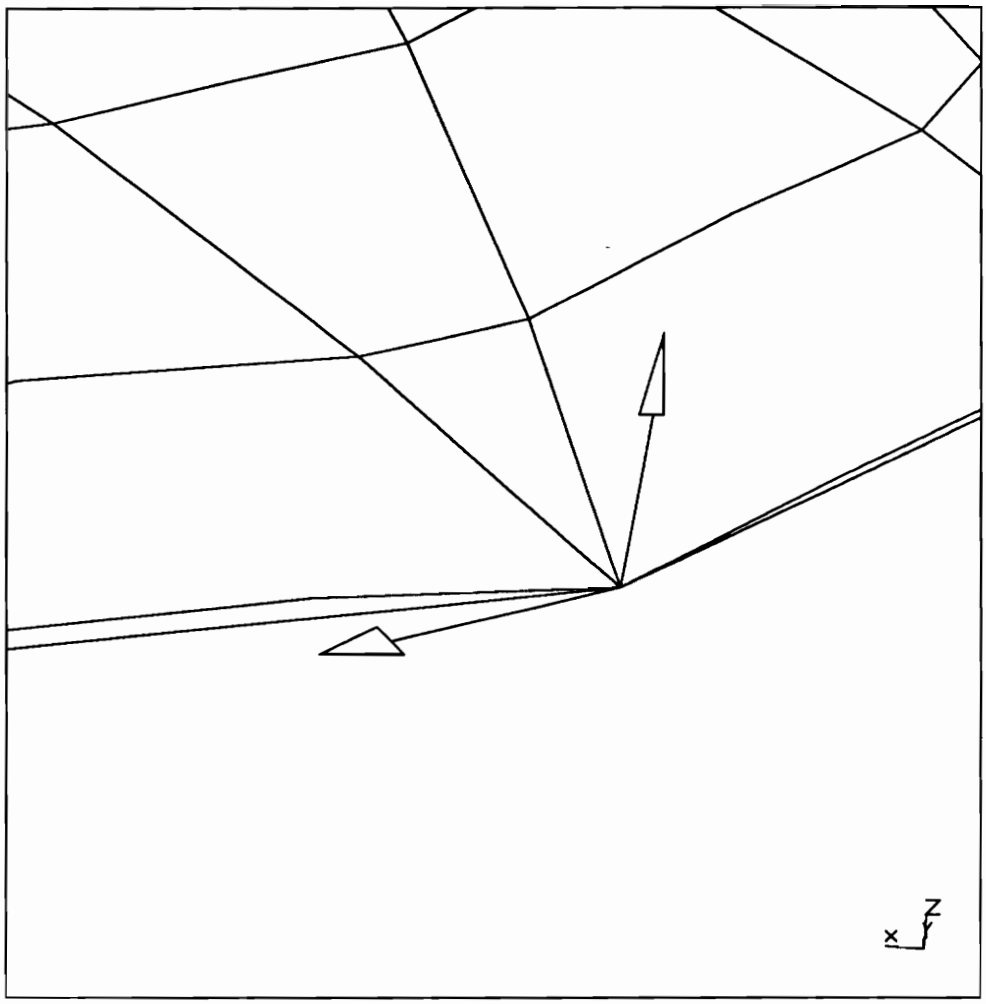

Fig. 2.8: Close-up view of a node where boundary conditions are applied

2.9 LOADS

2.9.1 Design Loads

The applied loads consist of dead and snow loads. The design dead load is 15 psf. The dead load consists of:

Grid framing:	2.76 psf
Decking:	5.0 psf
Connections	0.54 psf
Roofing:	1.5 psf
Insulation:	4.5 psf
Misc.	0.7 psf
	15.0 psf

The design snow load is 25 psf.

2.9.2 Load Discretization

Instead of using a computer program to discretize the loads as was done in [3], a more general graphical approach is used. This approach has the following advantages:

- **Can be used for different domes:** Since this method is graphical it is independent of the class of the dome and its geometry.
- **Can represent different loads:** This method allows the modeling of dead, snow and wind loads.

- **Can represent different load distributions:** Loads can be applied on arbitrary regions of the dome, which is useful for modeling snow and wind loads, which can have varying distributions.

The shell elements are used to distribute the loads to the connecting nodes. To discretize the loads, a linear analysis is performed with all the nodes in the model fixed. For the dead load the shell elements are subjected to a vertical body load of magnitude **(p_d / shell thickness)** where p_d is the pressure dead load. The resulting vertical reactions are then used as node loads for subsequent linear and nonlinear analyses (the other components of the reaction are very small and are therefore neglected).

Since snow loads are defined over a horizontal projection of the surface area of the dome, a pressure load p_L is applied to a flat area obtained by projecting the dome on a horizontal surface. The vertical reaction forces obtained from linear analysis are then applied at the dome nodes. To model snow loads over a particular area of the dome, loads are applied only to the shell elements defining that area.

Throughout this study, four load cases are considered:

1• Snow over entire dome (also referred to as uniform snow load).

2• Inner snow load (fig. 2.9).

3• Outes snow load (fig. 2.10).

4• Snow over half the dome (fig. 2.11).

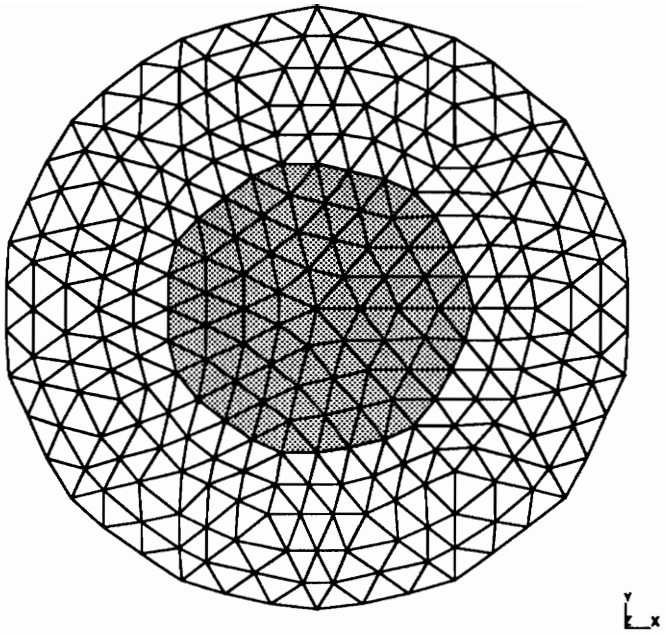

Fig. 2.9: Inner snow load.

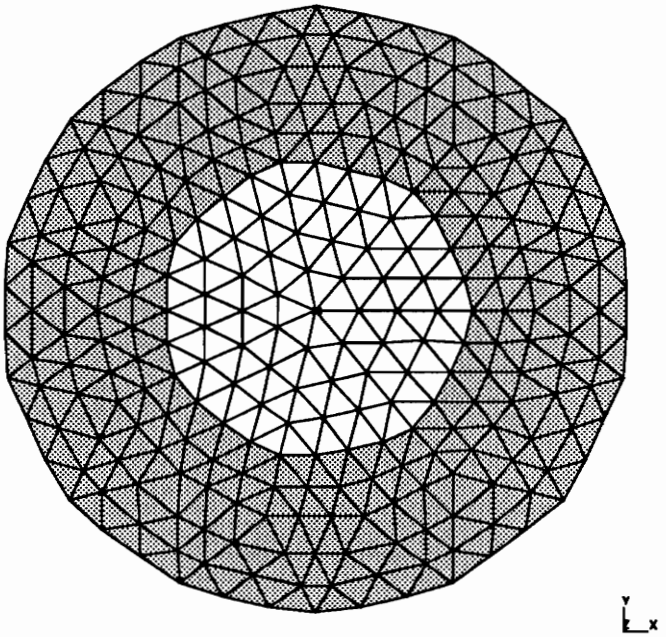

Fig. 2.10: Outer snow load.

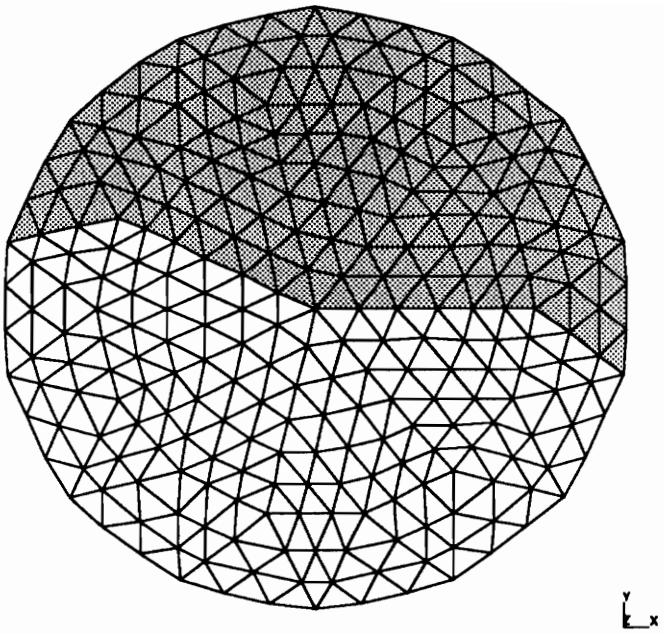

Fig. 2.11: Snow over half the dome.

3. LINEAR ANALYSIS OF THE DOME

3.1 PURPOSE

The main objectives of conducting linear analyses are to insure that the finite element model is free of defects and to obtain displacement and stress distributions to get an insight into behavior that can assist in nonlinear analyses. The dome model has to satisfy two important conditions:

- The response has to be symmetric for symmetric loads.
- Displacements should be reasonable (comparable to the displacements obtained for the Raleigh Triax dome [3, 7] since it is similar to the Varax dome in size and loading)

3.2 PROCEDURE

A linear analysis was conducted on ABAQUS with the shell elements removed (this greatly reduces the run time and memory needed). The displacements and maximum stresses (at the nodes) were monitored on one sector of the dome for symmetric load conditions. Four load cases were considered:

1- Uniform snow.

2- Inner snow load.

3- Outer snow load.

4- Snow over half the dome.

In each of the four cases the dead load was also included.

3.3 RESULTS

3.3.1 Uniform snow load

•*Displacements*

As shown on the displacement contours (fig. 3.1), the response is symmetric from one sector to the other. The maximum vertical displacement is 1.24 in at the nodes next to the apex, the vertical displacement at the apex is 1.22 in. The displacements are maximum near the apex, and minimum near the perimeter. The radial displacement at the ring nodes where the boundary conditions were applied is 0.40 in.

• *Stresses*

The stresses were determined at the nodes and the maximum values are shown in figure 3.2, negative stresses indicate compression whereas positive stresses indicate tension. The combined axial and bending stresses in the beam elements vary between 409.0 psi and 1244.0 psi. The distribution is such that the stress is maximum near the perimeter and then decreases to a minimum value near the apex. The shear stresses vary between zero and 145.0 psi with the same distribution as for the combined axial and bending stresses.

3.3.2 Inner snow load

•*Displacements:*

The maximum displacements are located under the snow load (fig. 3.3). The vertical displacement at the apex is 1.07 in and the radial displacement at the ring is 0.24-in. The response is also symmetric.

• *Stresses*

The combined axial and bending stresses are a minimum of 408.0 psi near the apex, then increase to a maximum of 1207.0 psi where the snow load ceases to be applied. The stresses then decrease towards the edges of the dome (fig. 3.4)

3.3.3 Outer snow load

•*Displacements:*

As was the case for inner snow load, the maximum displacements are located in the area where the snow load was applied (fig. 3.5). The vertical deflection at the apex is 0.64-in, whereas the radial displacement at the steel ring is 0.33-in.

• *Stresses*

The stresses are maximum under the snow load and are relatively low near the apex, 138.0 psi. The maximum combined axial and bending stresses are 1390.0 psi. Figure 3.6 shows the maximum stresses for the beams.

3.3.4 Snow over half the dome

•*Displacements:*

The displacements are maximum on the side where the snow load was applied (fig. 3.7). Maximum displacements of 1.36-in occurred near the apex. The vertical displacement at the apex is 0.79in, whereas the radial displacements at the steel ring vary between 0.19 and 0.35-in.

• *Stresses:*

Because of the nature of loading, the beams were subjected to more bending stresses than in the previous cases. Maximum stresses between 1200.0 and 1636.0 psi were located near the steel ring on the side where the load was applied. Stresses in the steel ring vary between 7020.0 and 12,875.0 psi.

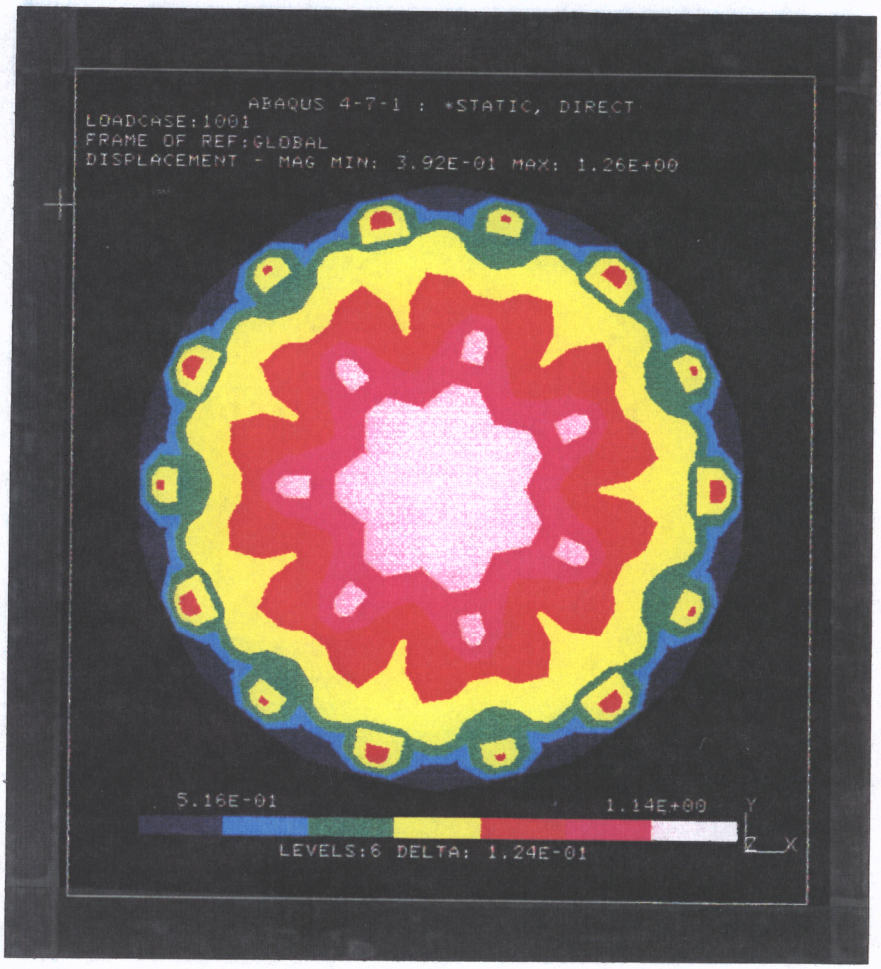

Fig. 3.1: Displacement contours for uniform snow load.

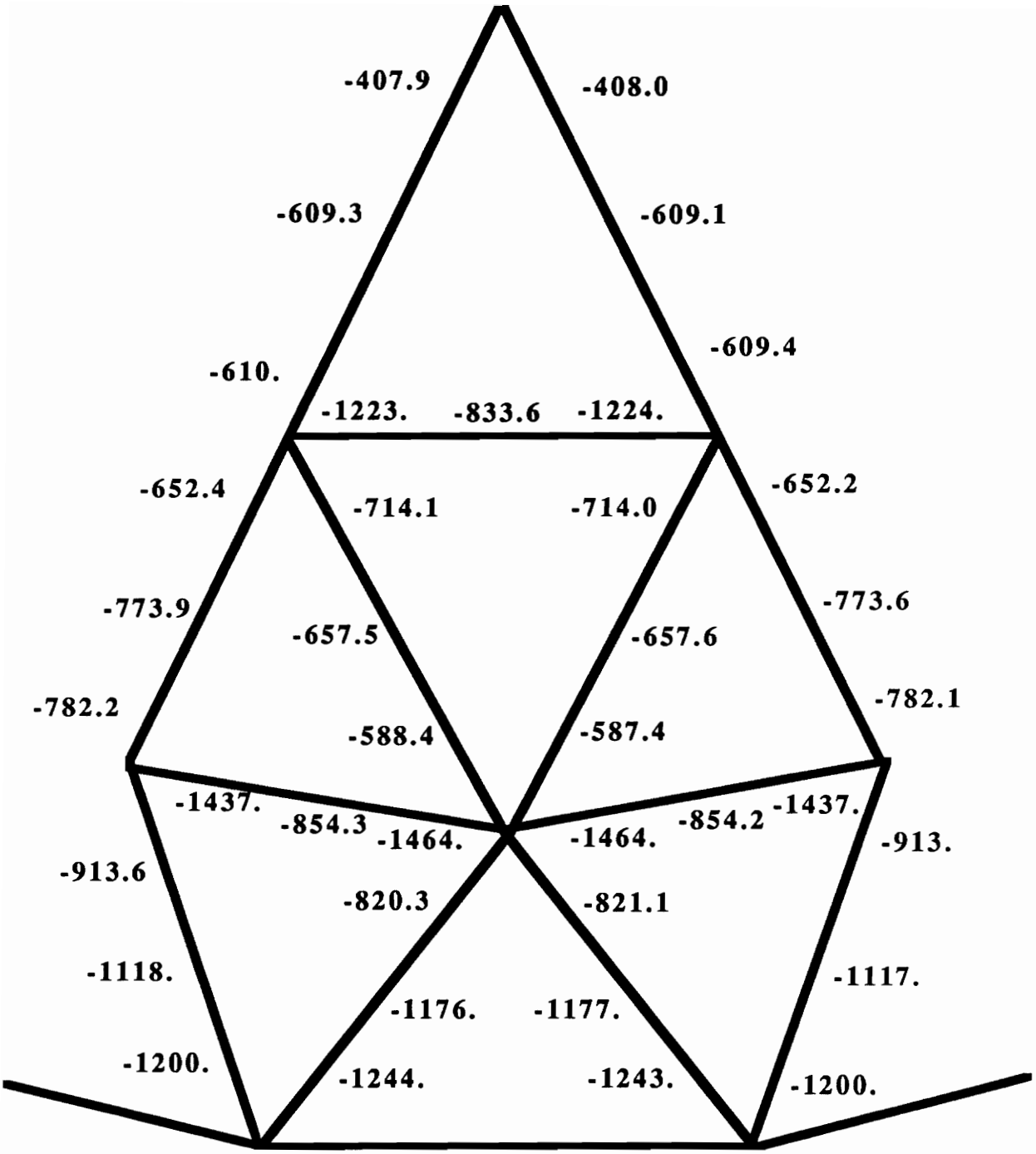

STRESS IN TENSION RING: 14527 psi

Fig. 3.2: Maximum combined axial and bending stresses for uniform snow.

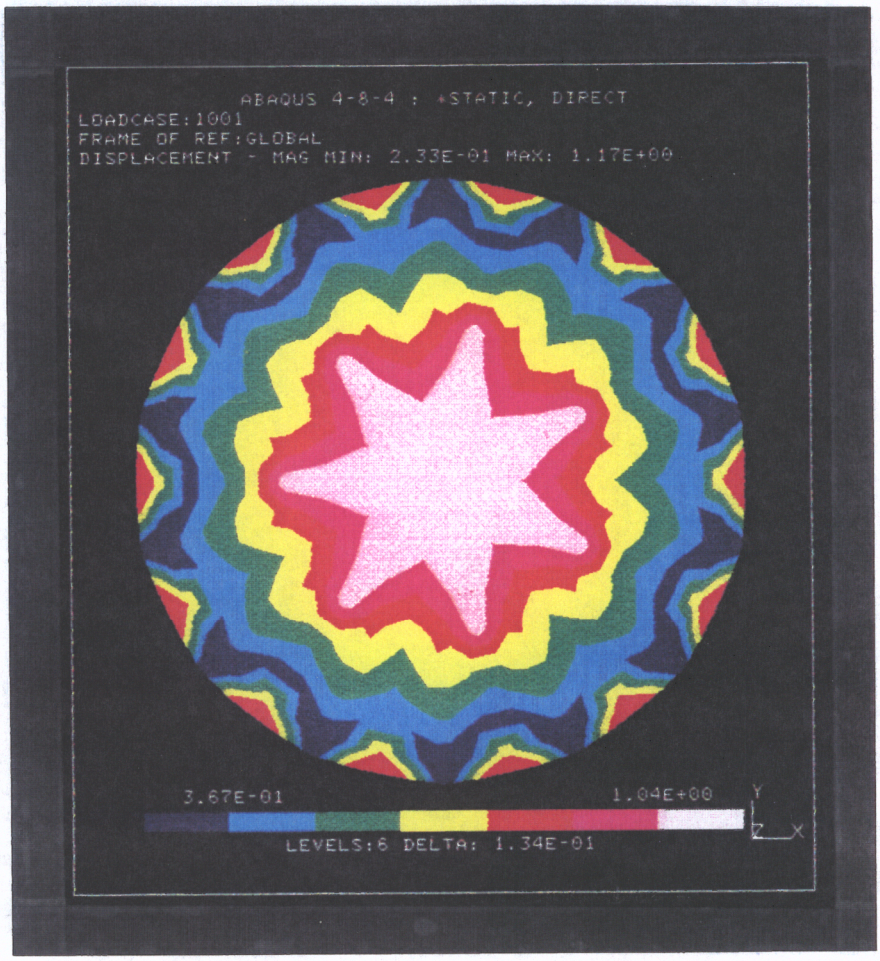

Fig. 3.3: Displacement contours for inner snow load.

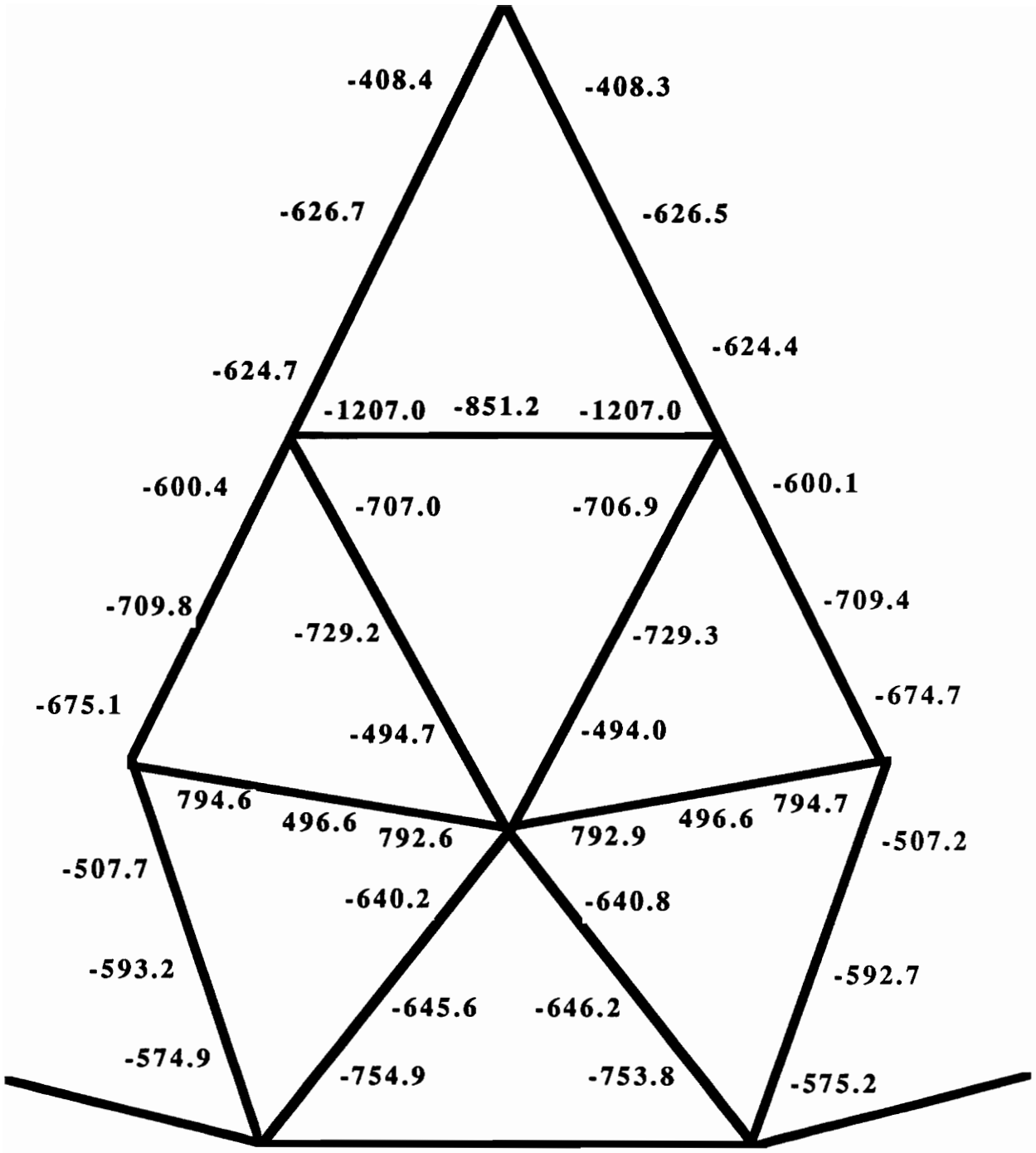

Fig. 3.4: Maximum combined axial and bending stresses for inner snow load

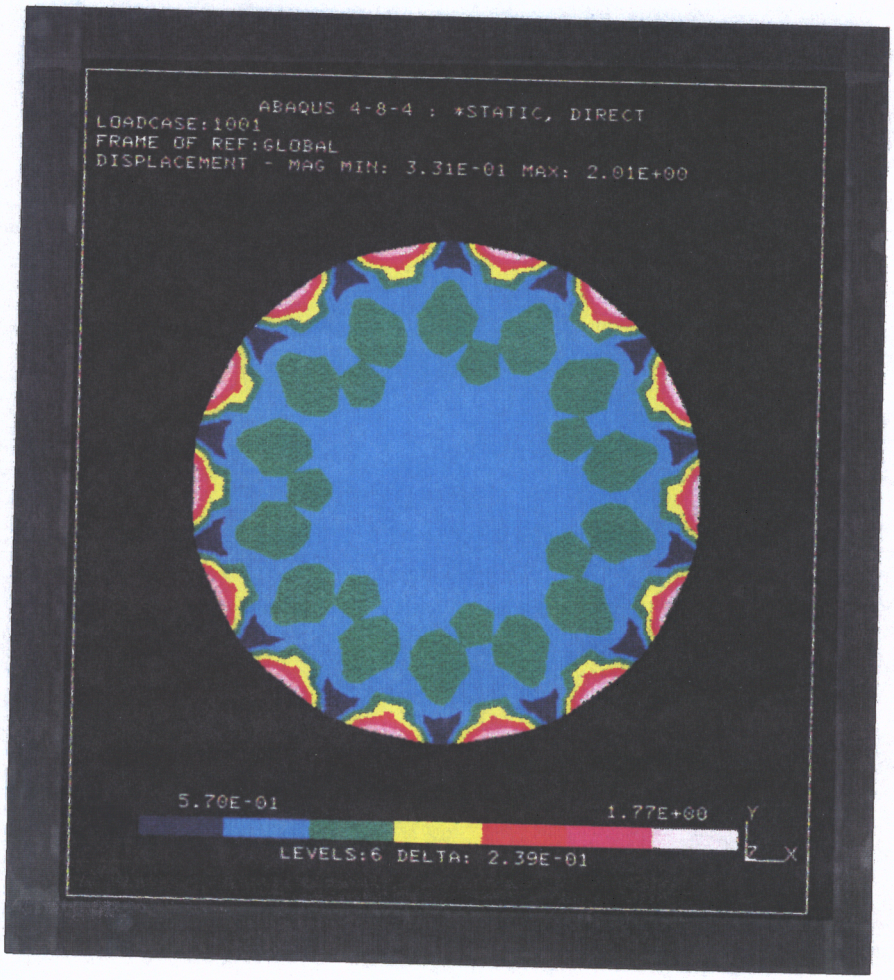

Fig. 3.5: Displacement contours for outer snow load.

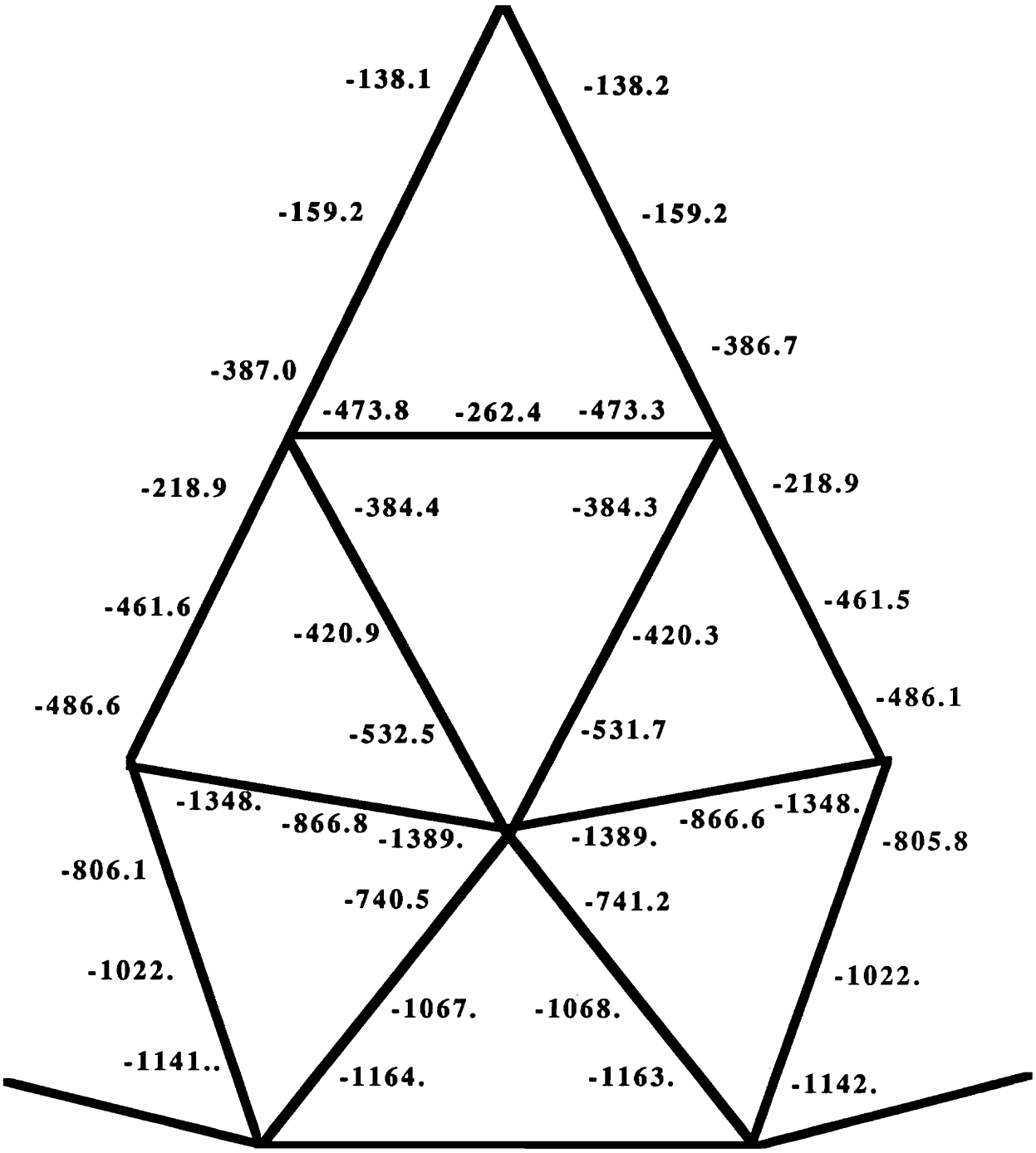

STRESS IN TENSION RING: 12322 psi

Fig. 3.6: Maximum combined axial and bending stresses for outer snow load

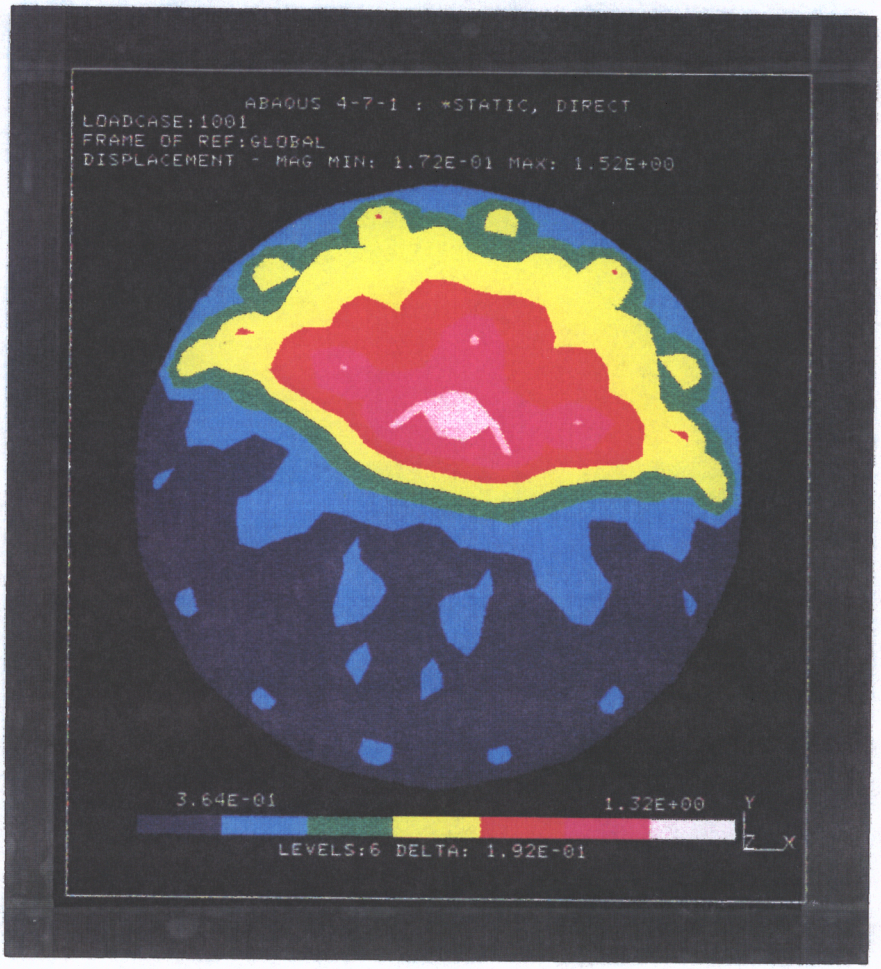

Fig. 3.7: Displacement contours for snow over half the dome.

4. NONLINEAR ANALYSIS OF THE DOME

4.1 PURPOSE

Geometrically nonlinear analysis was conducted to find the critical snow loads and to trace equilibrium paths to determine whether the critical load corresponds to a limit point or to a bifurcation point. In addition, buckling modes were determined. The maximum stresses at the beams were checked to determine if the material strength was exceeded since we assumed linearly elastic material behavior.

4.2 NONLINEAR ANALYSIS METHODS

Nonlinearities in a structure can be classified as material, related to a nonlinear stress-strain relationship, or geometric, where the strain-displacement relationship is nonlinear and equilibrium is satisfied for the deformed state. In this study only geometric nonlinearity is considered.

Nonlinear analysis is used to trace the equilibrium path up to and beyond the first critical point. As a result, we can determine the critical load at which the structure becomes unstable. The two methods used in this study are the modified Newton-Raphson method and the modified Riks-Wempner method.

The Newton-Raphson method [2, 9] starts with a known equilibrium point, and then uses iterative procedures to find the next equilibrium point at an increment of load $\Delta\lambda$. This procedure is repeated until the load approaches a limit point, where convergence becomes increasingly difficult. In the modified Newton-Raphson method, the stiffness matrix is not updated between iterations of a specified load increment to increase computational efficiency. Unlike the Newton-Raphson method, the modified Riks-Wempner method [9] can trace the equilibrium path beyond a limit point.

4.3 PROCEDURE

Nonlinear analysis was conducted with ABAQUS using:

1- The Newton-Raphson method to incrementally load the dome up to the full dead load (15 psf)

2- The Riks method to apply fractional increments of the snow load (25 psf) up to and beyond the critical point.

During the analysis the displacements and stresses at selected nodes and elements were monitored.

4.4 RESULTS

4.4.1 Uniform snow load

The dome exhibited instability when the snow load factor was 4.45 (snow load of 111.25 psf). The instability occurred at all the nodes simultaneously, which indicates global buckling of the structure. The vertical displacement at the apex at the critical load was about 3.7-in.

From the graph of the equilibrium path of some of the nodes (fig. 4.1), it appears that the failure corresponds to a bifurcation point (response is linear, then suddenly changes slope).

To determine the buckling mode, a deformed geometry plot was generated after the dome buckled. From the plot it can be concluded that the dome buckled by twisting about the Z axis (fig. 4.2). It should be noted that this buckling mode would probably be avoided if the effect of the decking was taken into consideration.

The maximum stresses before buckling were (fig. 4.3):

- **Axial and bending**

  compressive: 4866.0 psi at the beams near the perimeter.

  tensile: 3887.0 psi at the beams near the perimeter.

- **Shear :** 543.7 psi at the beams near the perimeter.

The maximum compressive stress is below the proportional limits of 5896.0 psi [3], whereas the tensile stresses is below the ultimate stress of 14500.0 psi

[3]. The shear stress was not critical since it is below the ultimate value of 1,510 psi [3].

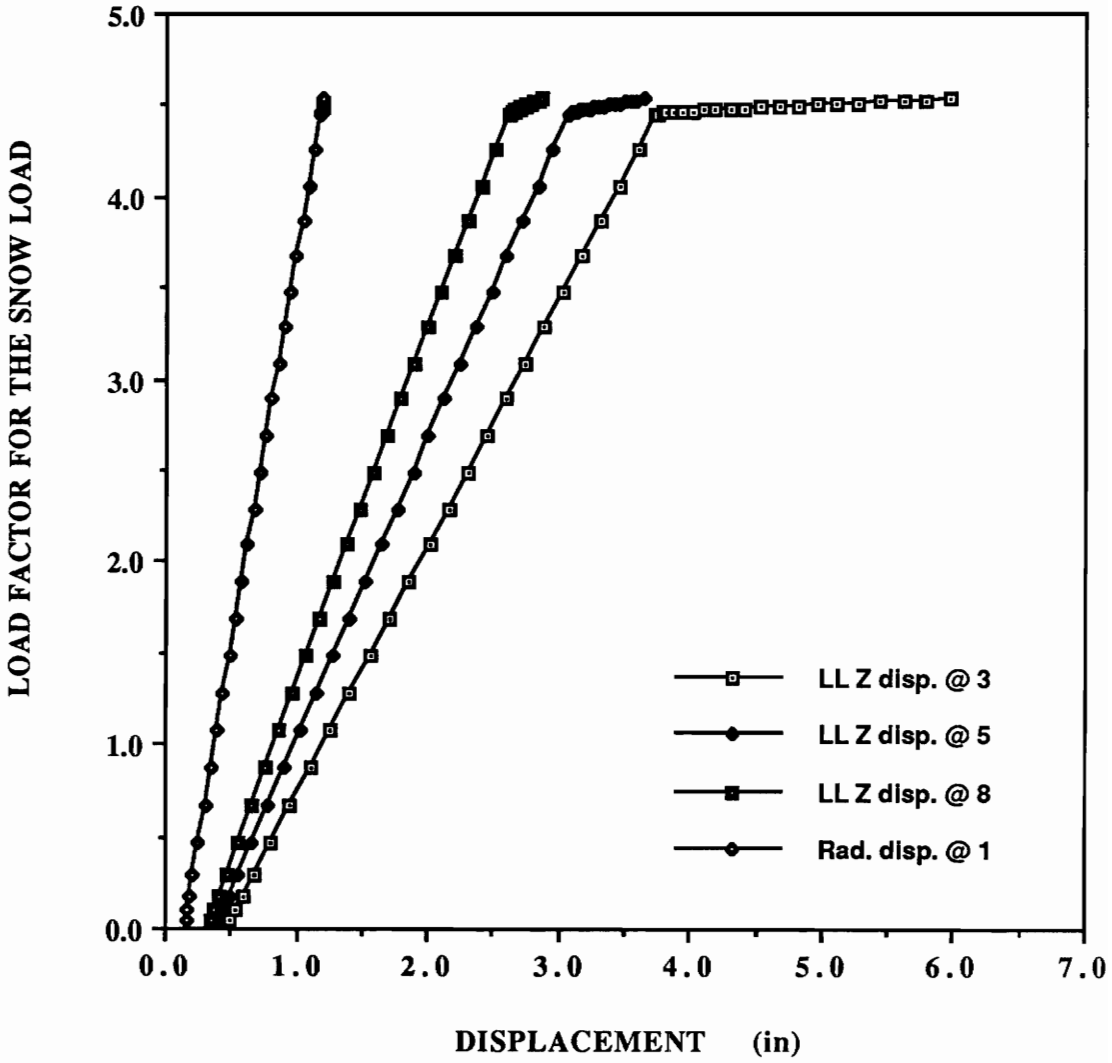

Fig. 4.1: Equilibrium paths at nodes 1, 3, 5, and 8 for uniform snow load.

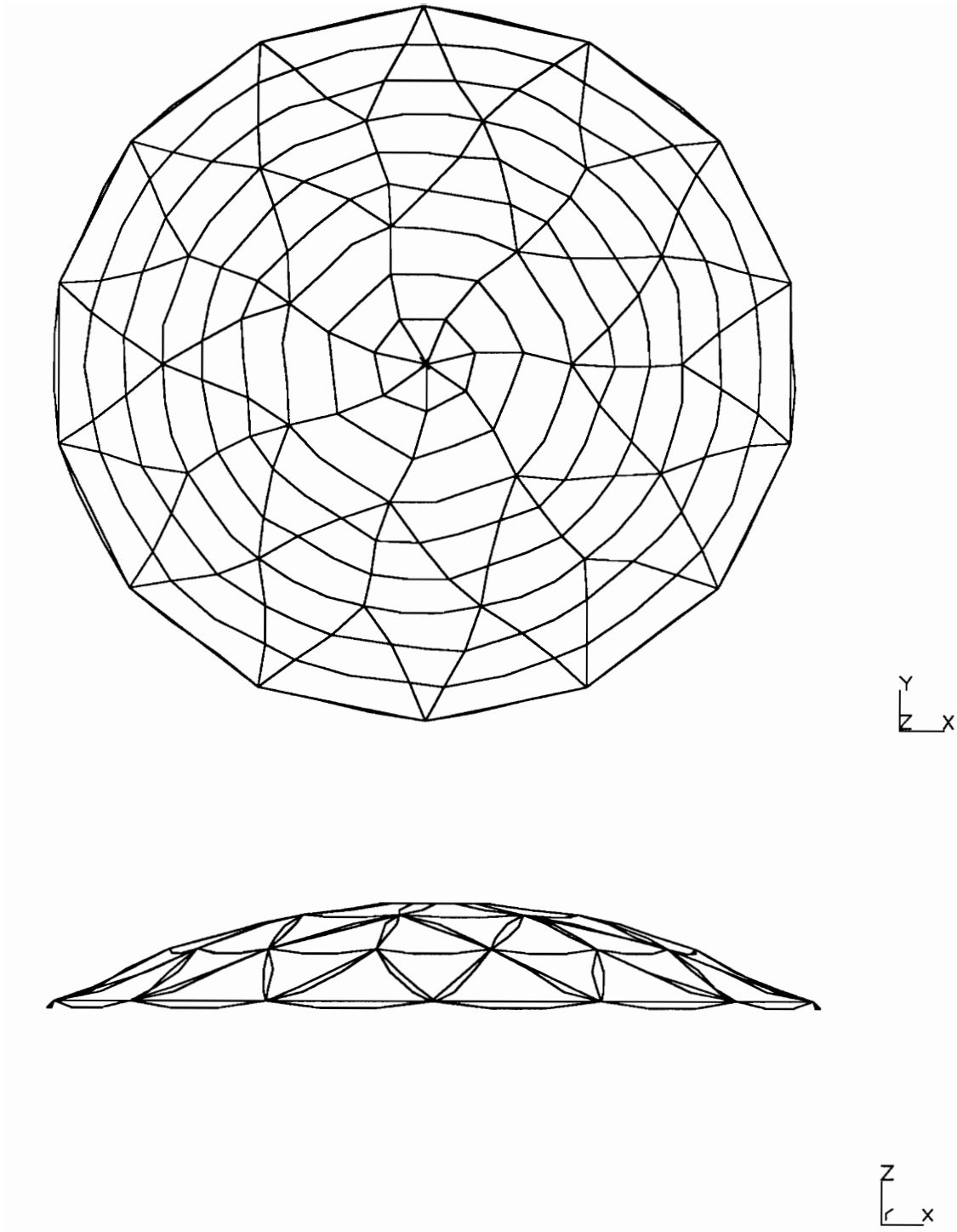

Fig. 4.2: Buckling mode for uniform snow load.

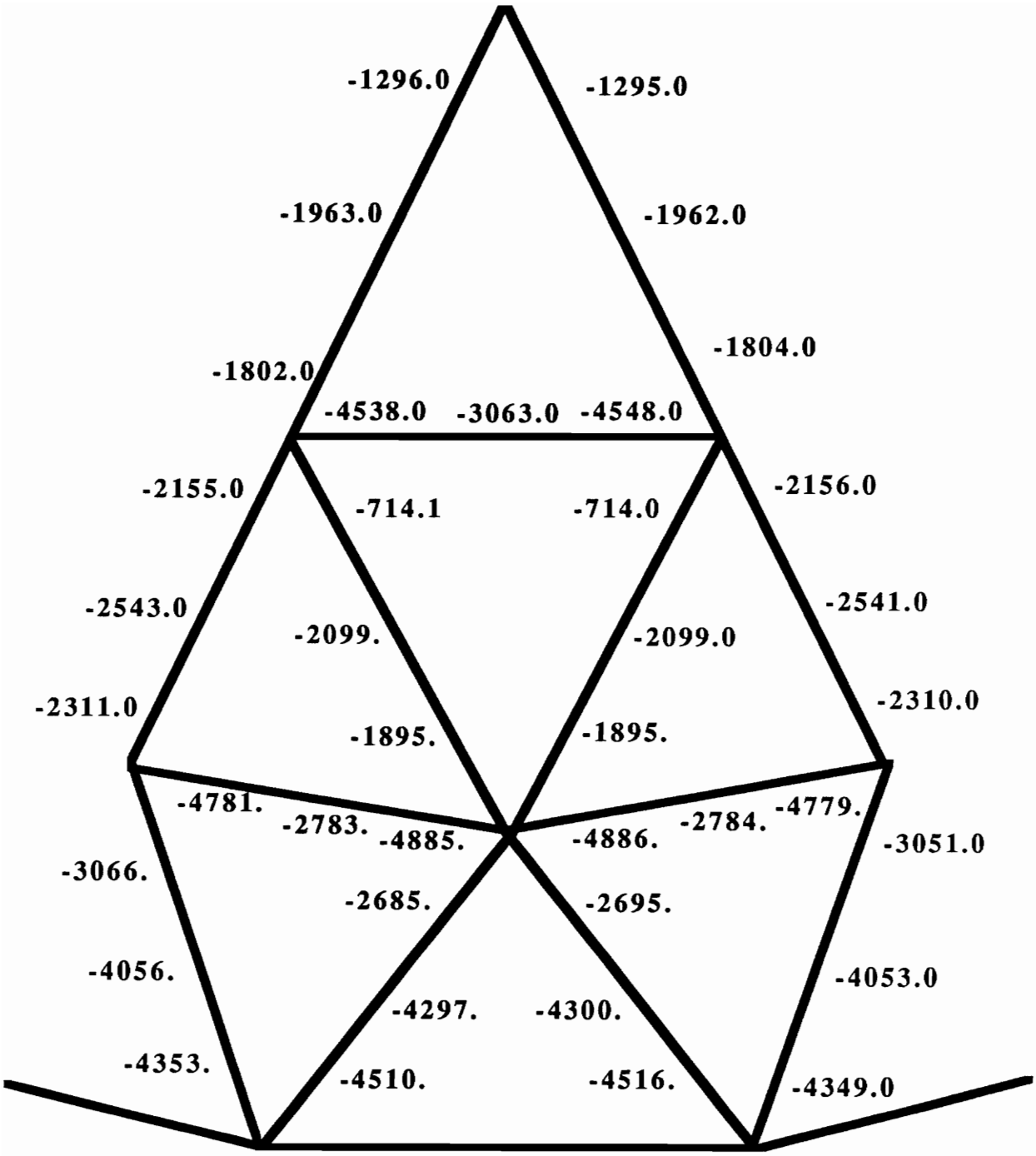

Fig. 4.3: Maximum stresses in beams just before buckling.

4.4.2 Inner snow load

The second load distribution considered was inner snow load. The dome was unstable at a snow load factor of 4.62. The vertical displacement at the apex just before buckling is 3.3-in.

As shown in the deformed geometry plot (fig. 4.4), the dome experiences local buckling in the beams under the snow load (first ring).

The equilibrium paths for nodes far from where buckling occurs (fig. 4.5) are nearly straight and do not exhibit any instability; however, equilibrium paths for nodes of the buckled beams change slope or direction at the critical load (figs. 4.6, 4.7).

The maximum stresses before buckling were (fig. 4.8):

- **Axial and bending**

  compressive: 4825.0 psi at the beams on the first ring.

  tensile: 3060.0 psi at the beams on the first ring.

- **Shear :** 303.0 psi.

The compressive stresses do not exceed the proportional limit.

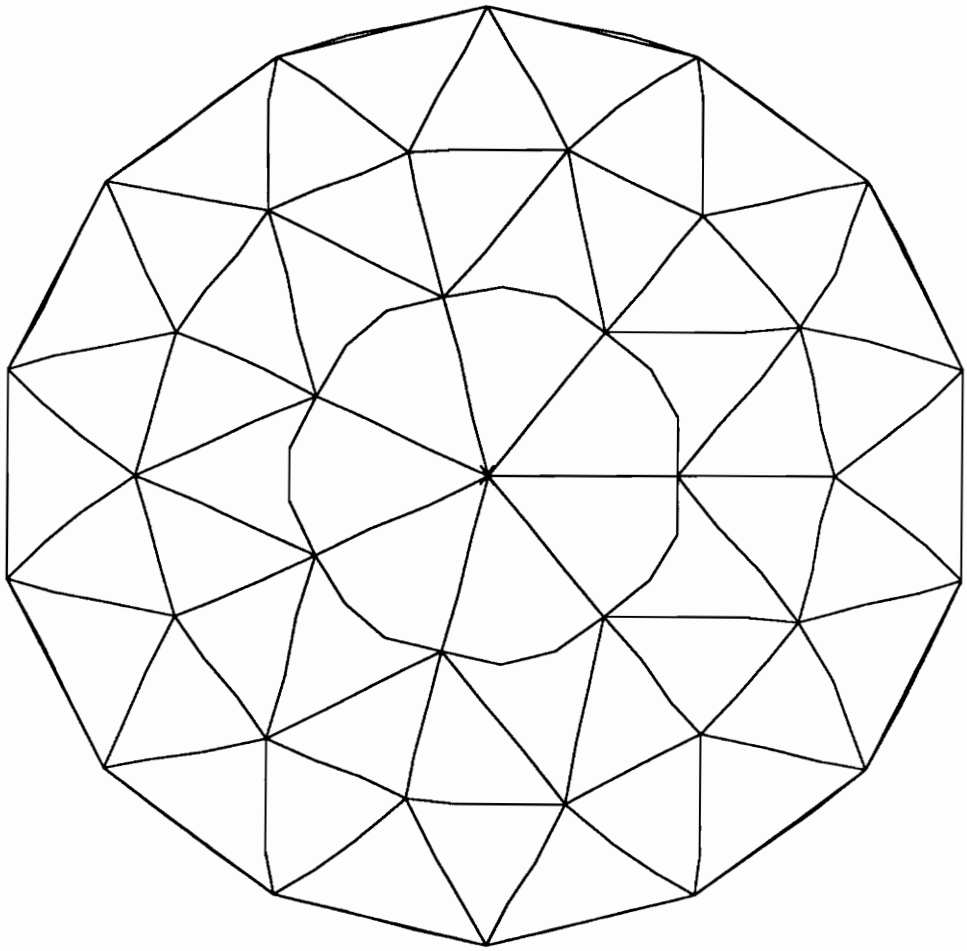

Fig. 4.4: Buckled shape for inner snow load.

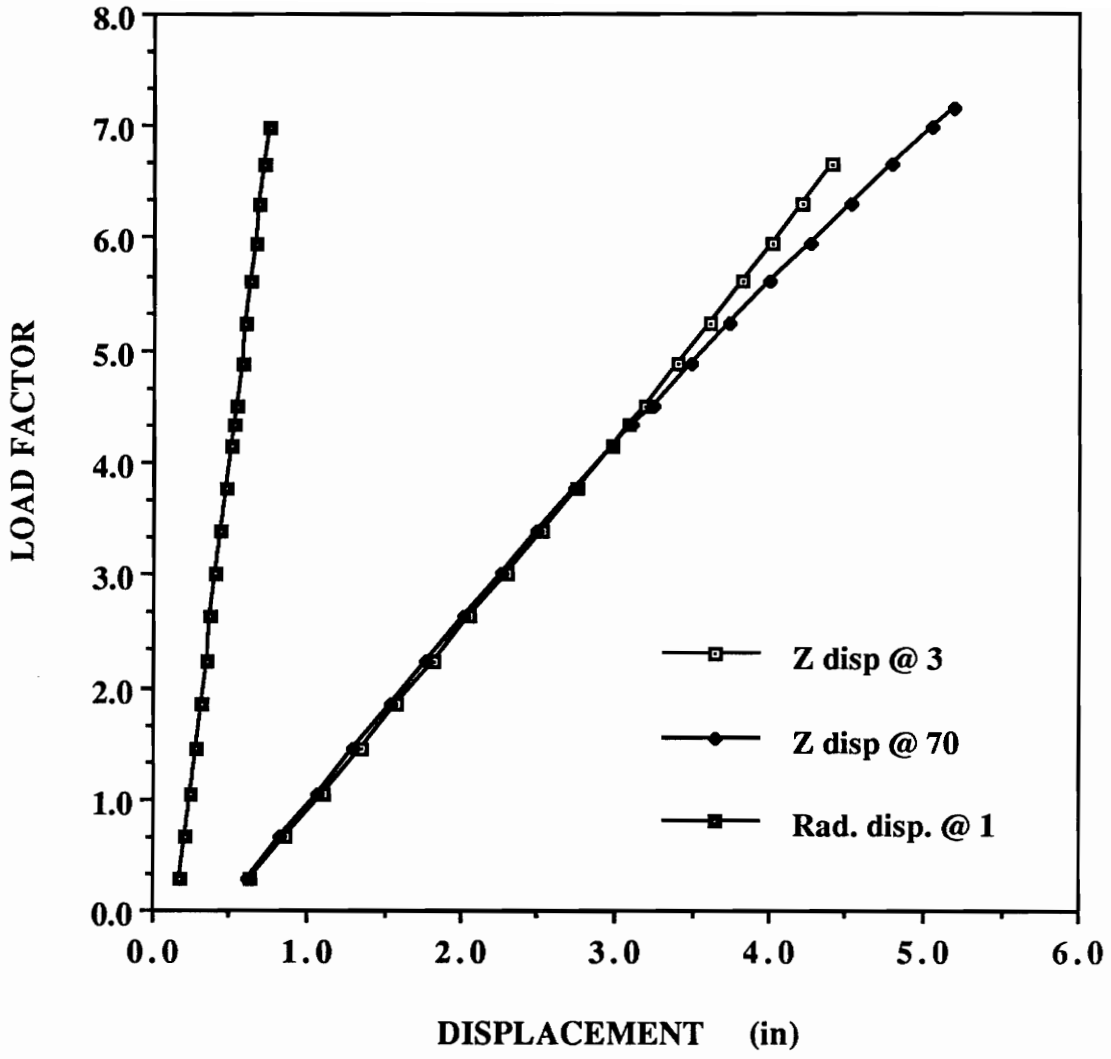

Fig. 4.5: Equilibrium paths at the apex (3), steel ring (1) and node 70.

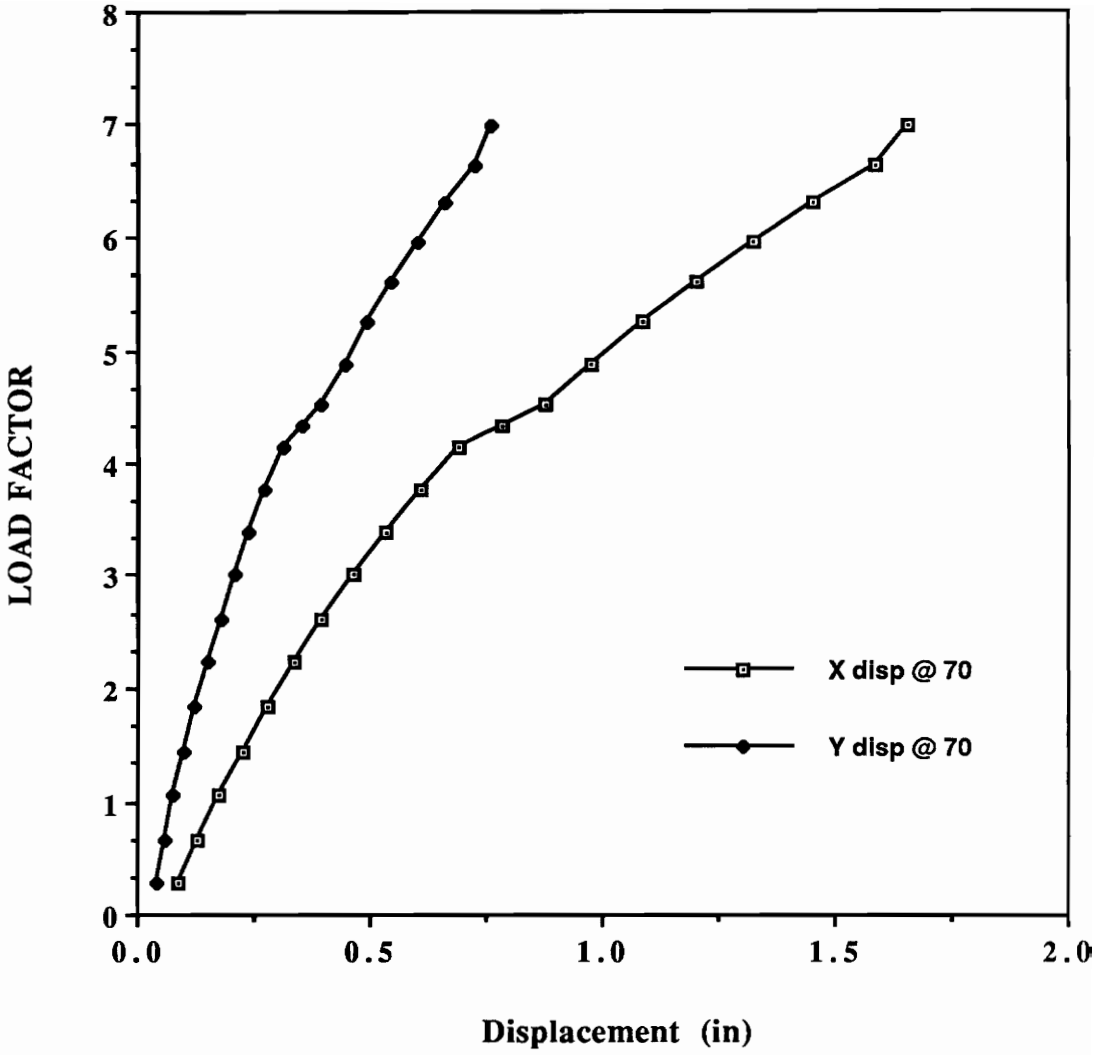

Fig. 4.6: Equilibrium paths for lateral displacements at node 70.

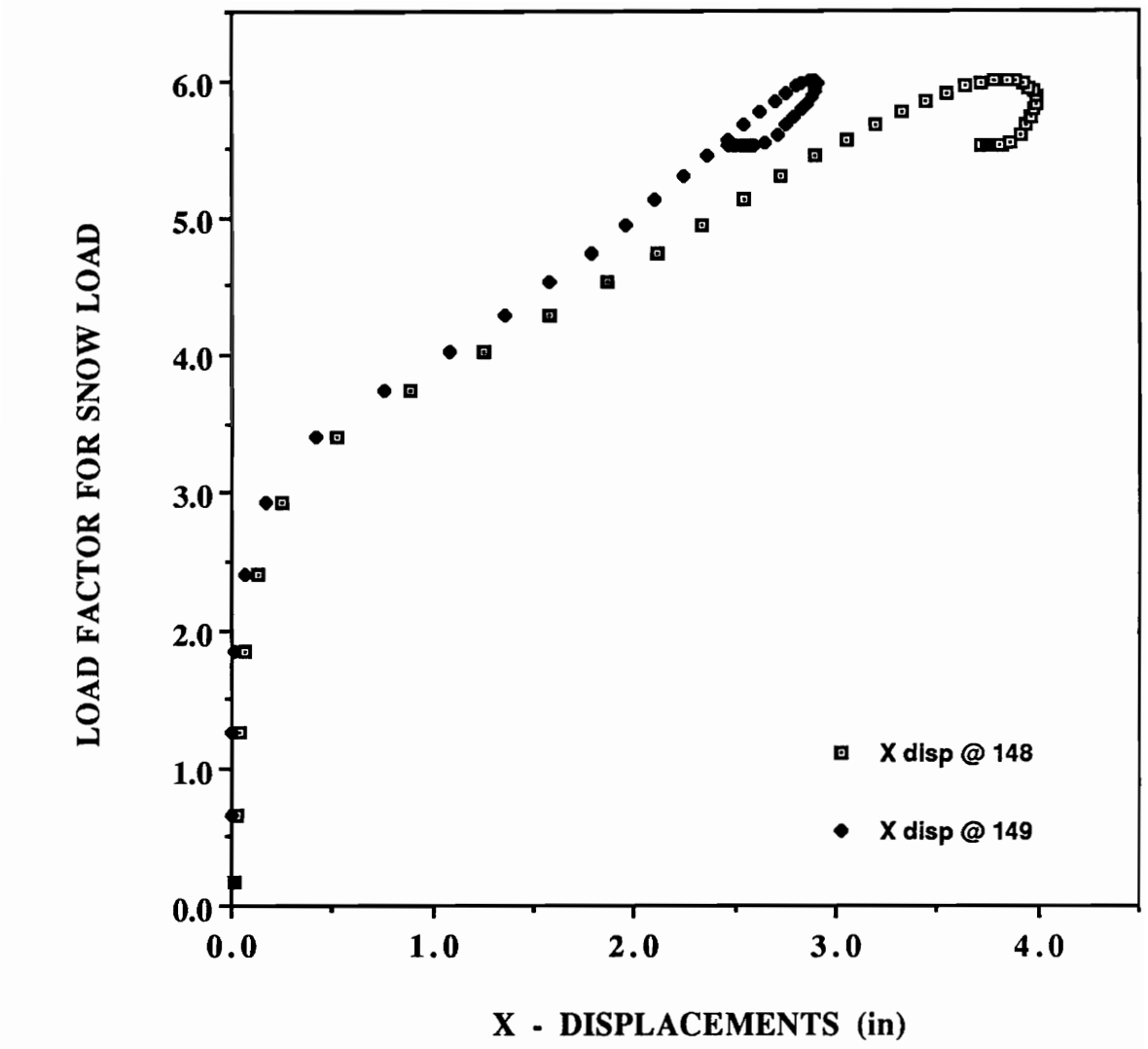

Fig. 4.7: Equilibrium paths for nodes 148 and 149.

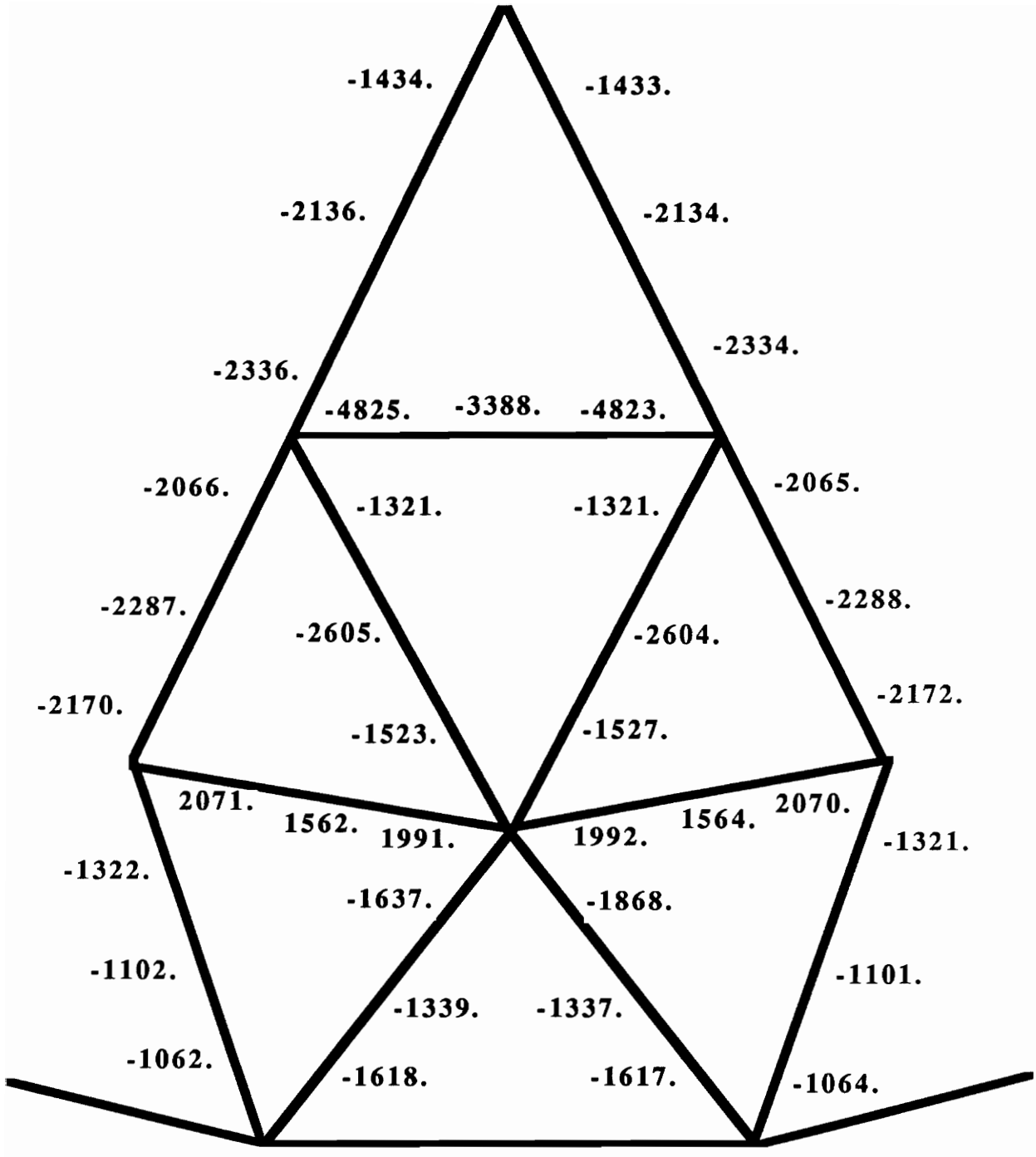

Fig. 4.8: Maximum stresses just before buckling for inner snow load.

4.4.3 Outer snow load

The critical snow load factor for outer snow load was 5.55. Both buckling mode (fig. 4.9) and equilibrium paths (fig. 4.10)are similar to the uniform snow load case. However, the failure mode was more localized. Only the beams where snow load was applied buckled. The vertical deflection at the apex just before buckling is 1.3-in, whereas the radial displacement at the perimeter is 1.1-in.

The maximum stresses before buckling were (fig 4.11):

- **Axial and bending**

  compressive: 7485.0 psi at the beams near the perimeter.

  tensile: 4931.0 psi at the beams near the perimeter.

- **Shear :** 572.0 psi.

Although the maximum compressive stress is below the ultimate value of 8470.0 psi [3], it exceeds the proportional limit of 5896.0 psi. This indicates that material nonlinearities need to be considered.

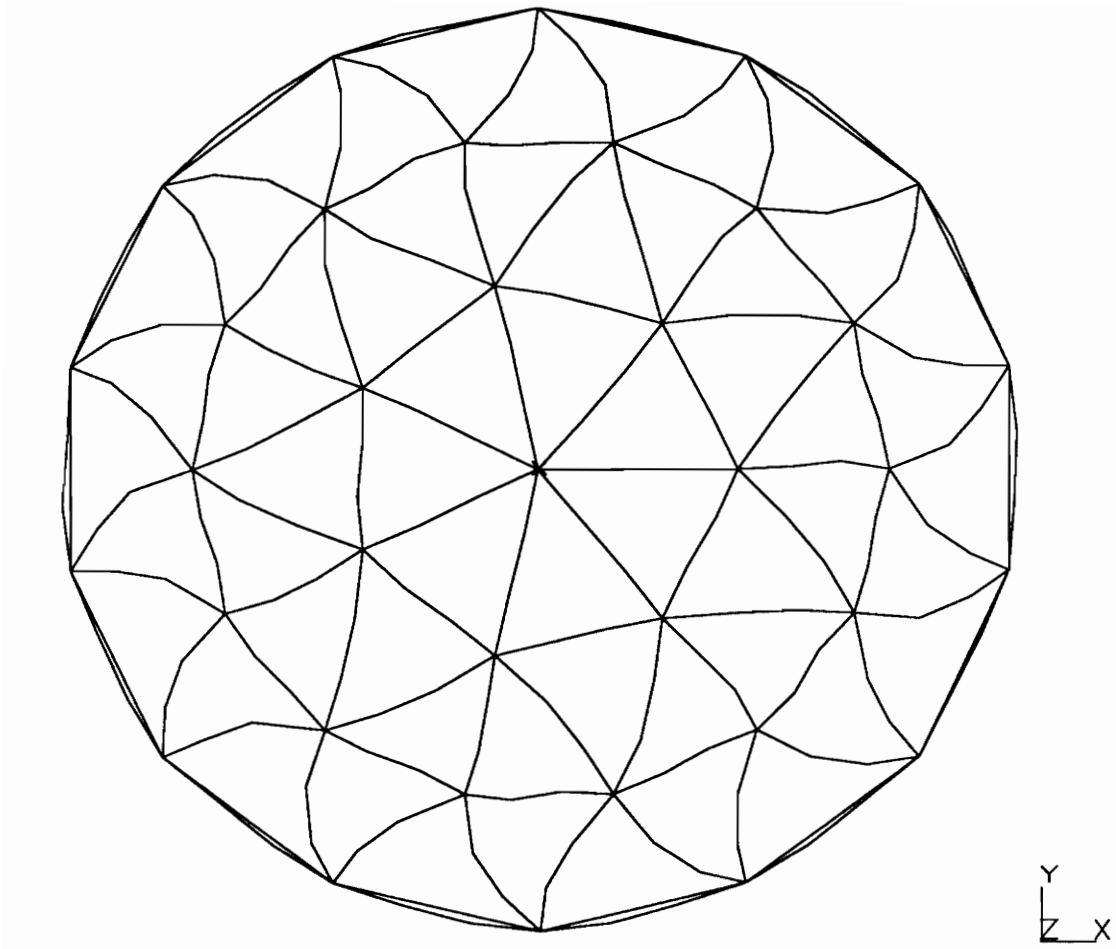

Fig. 4.9: Buckling mode for outer snow load.

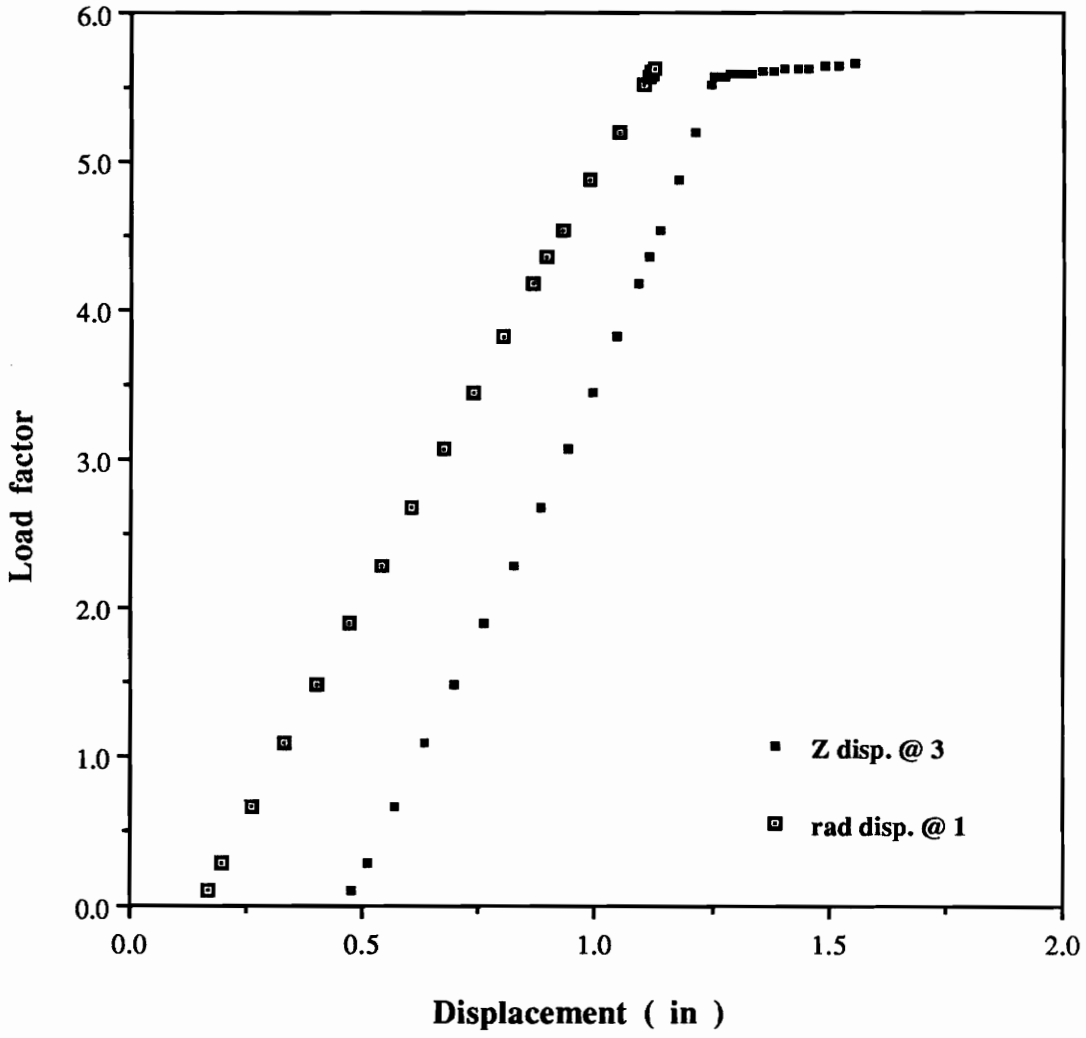

Fig. 4.10: Equilibrium paths at the apex (3) and steel ring (1) for outer snow load.

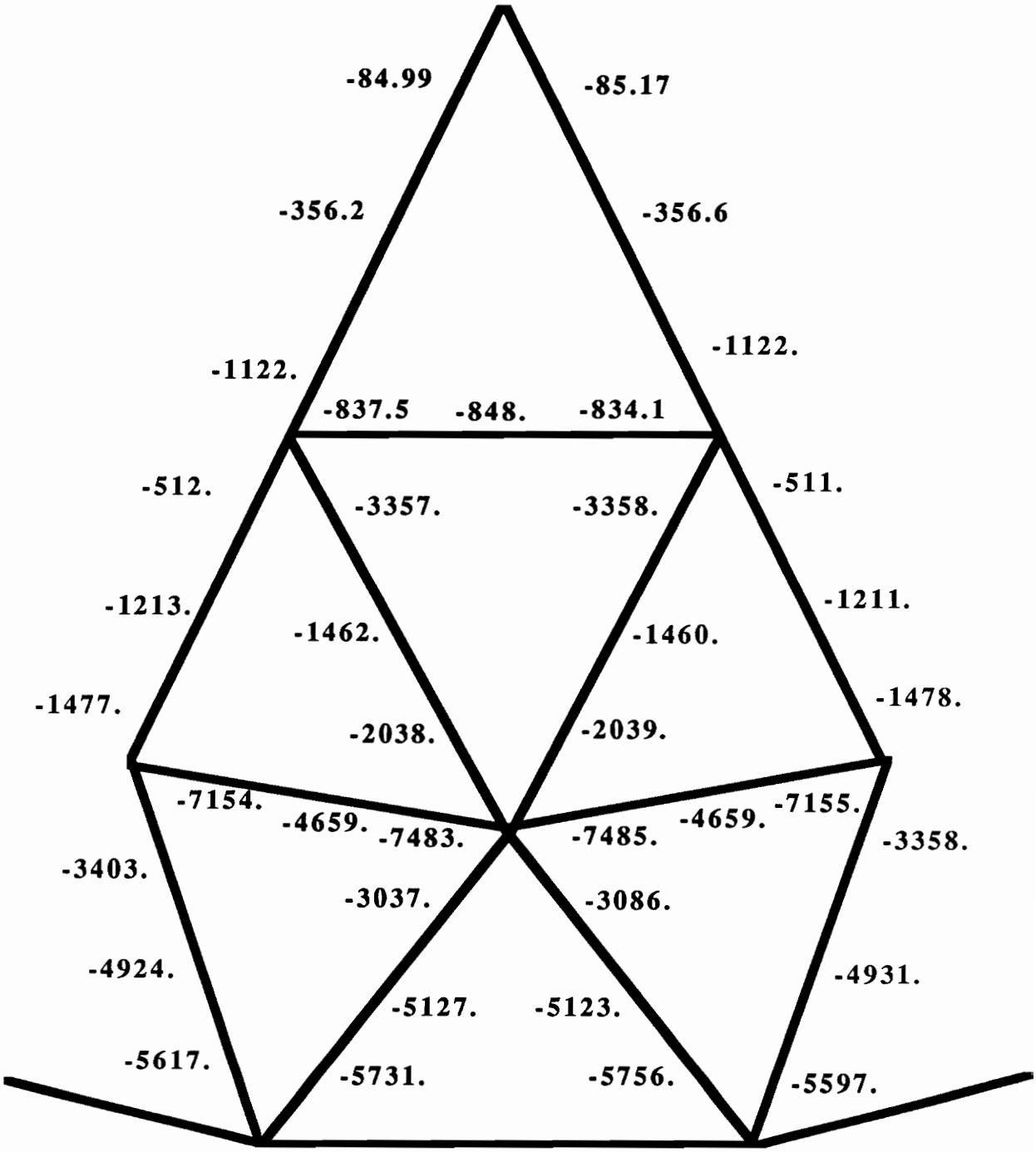

Fig. 4.11: Maximum stresses just before buckling for outer snow load.

4.4.4 Snow over half the dome

The critical load factor was about 6.0, which is relatively high. From the buckled shape (fig. 4.12), it appears that buckling was local and was limited to one beam element in the region where the snow load was applied.

The equilibrium paths (figs. 4.13, 4.14) indicate that instability corresponds to a limit point.

The maximum stresses before buckling were:

- **Axial and bending**

  compressive: 34,493.0 psi at the beam which buckled.

  tensile: 38,711.0 psi at the beam which buckled.

- **Shear :** 1774.0 psi.

All of these maximum stresses were located in the beam that experienced buckling. These stresses exceed the ultimate stresses by a large margin.

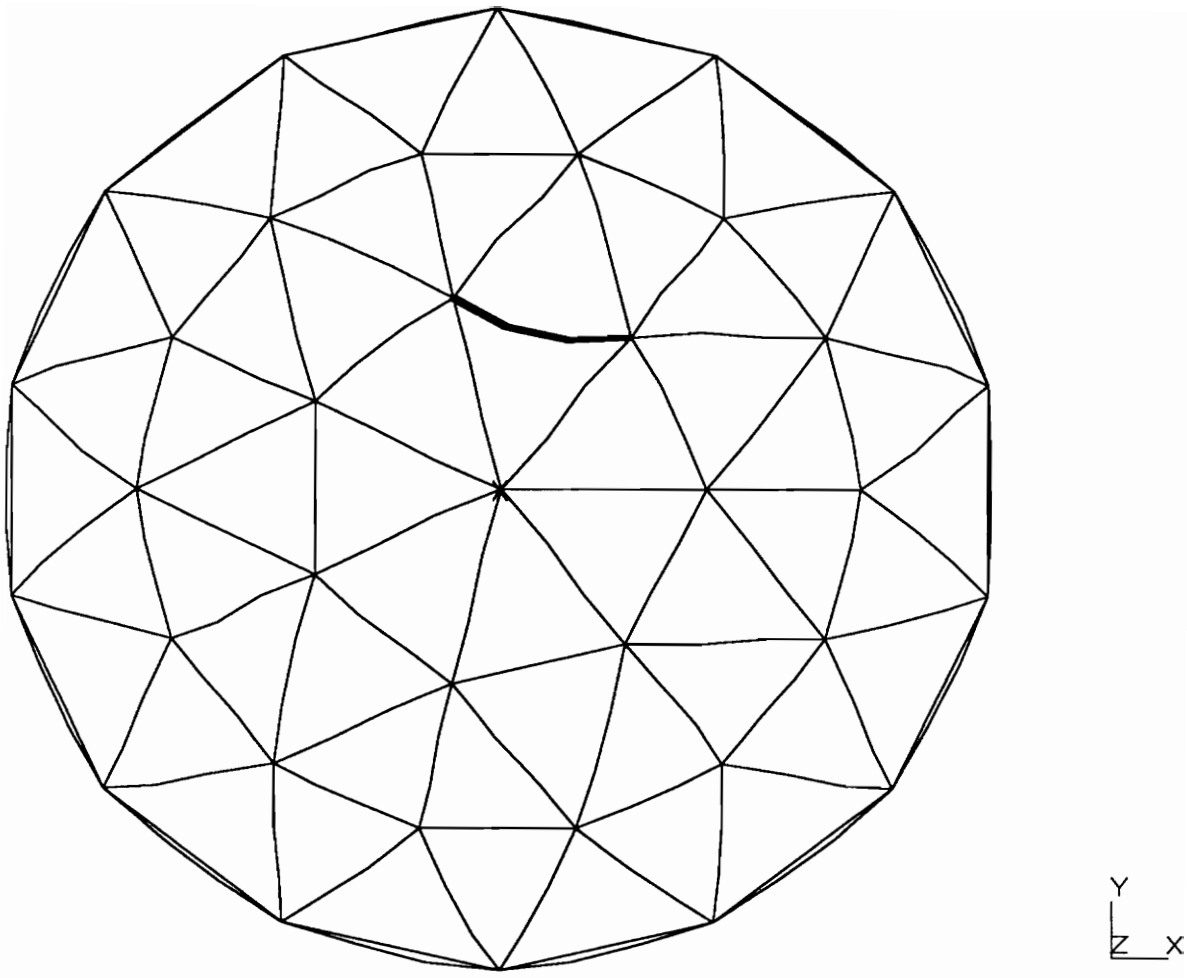

Fig. 4.12: Buckling mode for snow over half the dome.

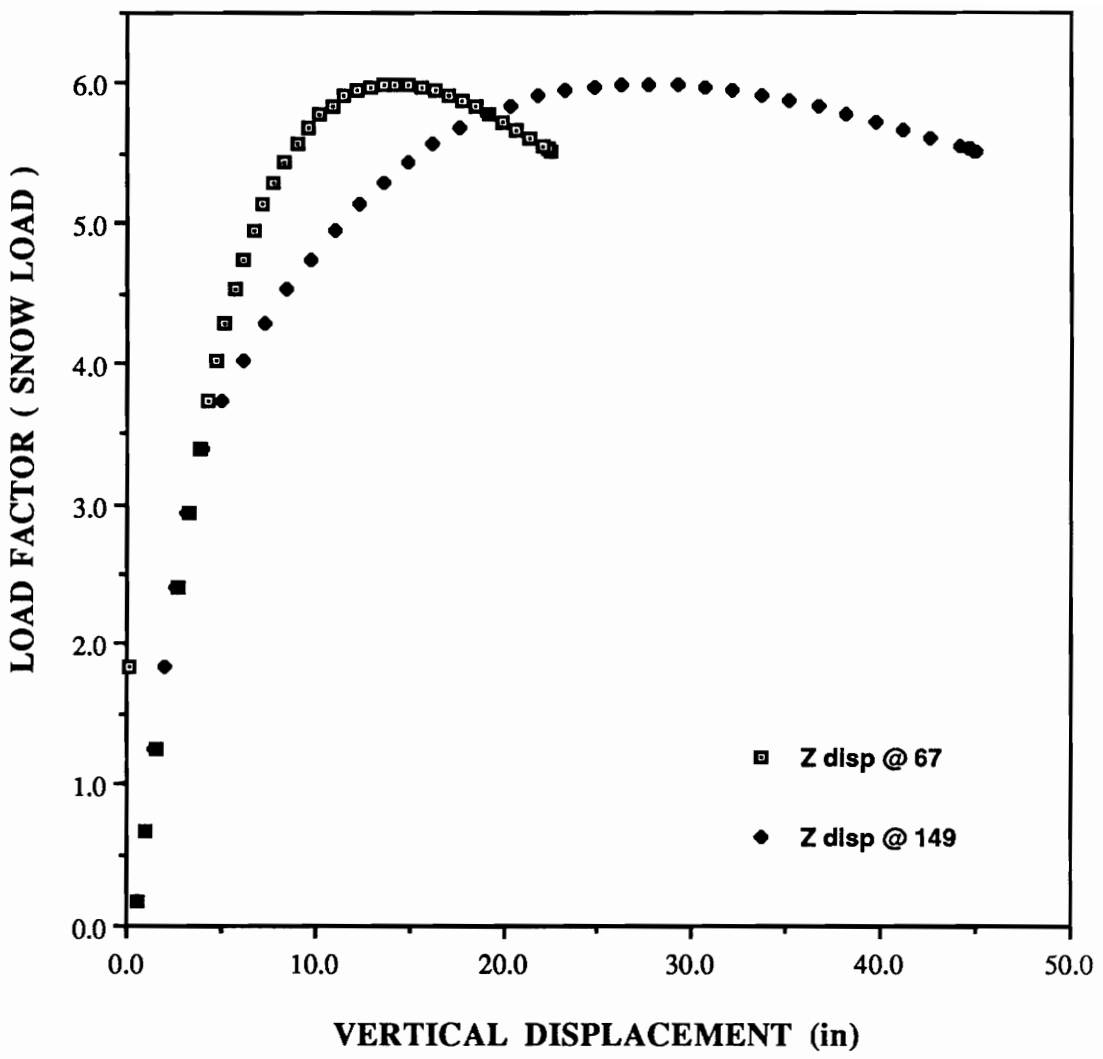

Fig. 4.13: Equilibrium paths at nodes 67 and 149.

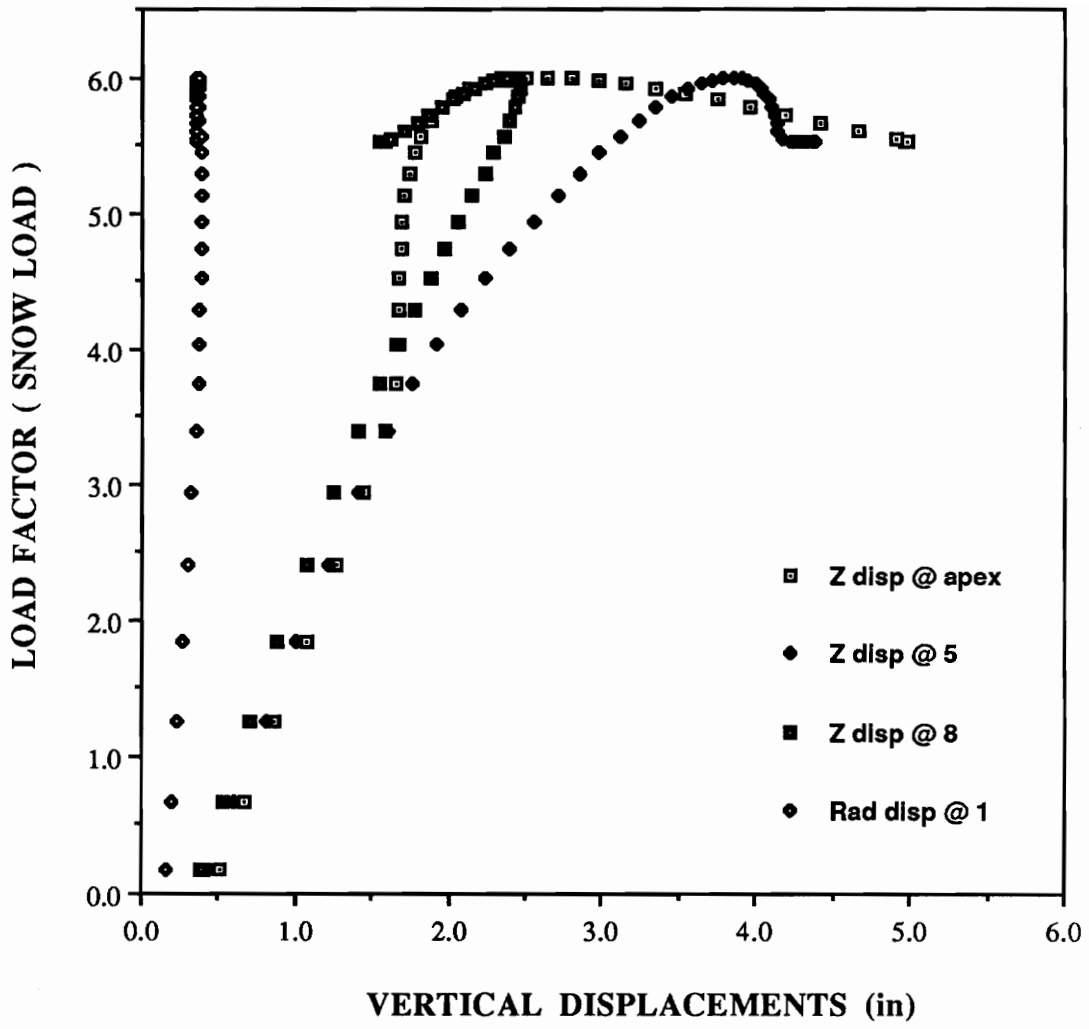

Fig. 4.14: Equilibrium paths for nodes 1, 3, 5 and 8.

5. COMBINED LINEAR AND NONLINEAR ANALYSIS

5.1 OVERVIEW

Combined linear and nonlinear analysis can be a useful tool for predicting the critical load and mode for different load cases. One disadvantage of nonlinear analysis is that the critical load is not known beforehand; therefore judgement has to be used to predict a stopping point for the analysis. By conducting combined linear and nonlinear analysis, the critical load can be predicted and nonlinear analysis can be stopped shortly after the structure becomes unstable. Another advantage of combined linear and nonlinear analysis is its low cost compared to nonlinear analysis, especially if the critical load can be predicted for small base loads. In this section, combined linear and nonlinear analysis is conducted for the load cases considered so far. The results are compared to the results obtained by nonlinear analysis and the suitability of the method is investigated.

5.2 PROCEDURE

The critical load is determined by interpolating or extrapolating from two or more runs. The procedure includes three steps:

1• Conduct nonlinear analysis for a base load (${}^{b}p$) consisting of a "dead" load and a multiple of the "live" load.

$$ {}^{b}p = p_D + {}^{b}\lambda\, p_L \qquad (5.2.1) $$

2• compute and store the tangent stiffness matrix ${}^{b}K$.

3• Conduct nonlinear analysis for reference load plus a fraction of the live load ($\beta\, p_L$). ABAQUS recommends that 1% of the predicted critical load be used; however, judgement has to be used, at least for the first attempt.

$$ {}^{r}p = {}^{b}p + \beta\, p_L \qquad (5.2.2) $$

From the analysis we can determine the tangent stiffness matrix ${}^{r}K$ at the reference load ${}^{r}p$. Also, the change in stiffness, ΔK, from ${}^{b}p$ to ${}^{r}p$ is determined.

$$ \Delta K = {}^{r}K - {}^{b}K \qquad (5.2.3) $$

4• The linear buckling hypothesis suggests that:

if

$$ p = {}^{b}p + \Delta\lambda\, p_L \qquad (5.2.4) $$

then

$$ K = {}^{b}K + \Delta\lambda\, \Delta K \qquad (5.2.5) $$

At the critical load, **K** is singular, i.e., det **K** = 0, which corresponds to the eigenvalue problem:

$$[\,{}^{b}\mathbf{K} + \Delta\lambda\, \Delta\mathbf{K}\,]\, \Delta\mathbf{q} = \mathbf{0} \qquad (5.2.6)$$

The solution to the previous equation yields a number of eigenvalues $\Delta\lambda$ and the corresponding buckling mode shapes. The critical eigenvalue is the smallest eigenvalue found.

Analysis with ABAQUS

The base load consists of the dead load and a multiple of the live load (Equation 5.2.7). The load increment is equal to a fraction of the live load (Equation 5.2.8).

$$\mathbf{{}^{b}p} = \mathbf{p_D} + {}^{b}\lambda\, \mathbf{p_L} \qquad (5.2.7)$$

$$\mathbf{p_j} = \beta\, \mathbf{p_L} \qquad (5.2.8)$$

The applied load used to determine $\Delta\mathbf{K}$ is expressed as:

$$\mathbf{p} = \mathbf{{}^{b}p} + C\, \mathbf{p_j} \qquad (5.2.9)$$

The critical load is then expressed as:

$$\mathbf{p_{cr}} = \mathbf{{}^{b}p} + C_{cr}\, \mathbf{p_j} \qquad (5.2.10)$$

Replacing $\mathbf{{}^{b}p}$ and $\mathbf{p_j}$ by their values from equations (5.2.7) and (5.2.8), respectively, we obtain the expression for the critical load:

$$\mathbf{p_{cr}} = \mathbf{p_D} + (\, {}^{b}\lambda + C_{cr}\, \beta\,)\, \mathbf{p_L} \qquad (5.2.11)$$

Letting $\Delta\lambda_{cr} = C_{cr}$ and ${}^{b}\lambda_{cr} = {}^{b}\lambda + \Delta\lambda_{cr}\,\beta$, the critical load becomes:

$$P_{cr} = p_D + {}^{b}\lambda_{cr}\, p_L \qquad (5.2.12)$$

5.3 RESULTS OF THE ANALYSES

Combined linear and nonlinear buckling analyses were conducted for uniform snow load, inner snow load, outer snow load, and load over half the dome. The critical live load factors are determined for various base loads and the results are plotted in a $\lambda - {}^{b}\lambda$ graph to be compared with the results obtained by nonlinear analysis. Figure 5.1 illustrates the procedure. The 45° line ($\lambda = {}^{b}\lambda$) passes through the critical load factor. The critical load prediction curve is defined by the collection of (${}^{b}\lambda$, ${}^{b}\lambda_{cr}$) points, where each critical load factor ${}^{b}\lambda_{cr}$ corresponds to a base load ${}^{b}\lambda$..

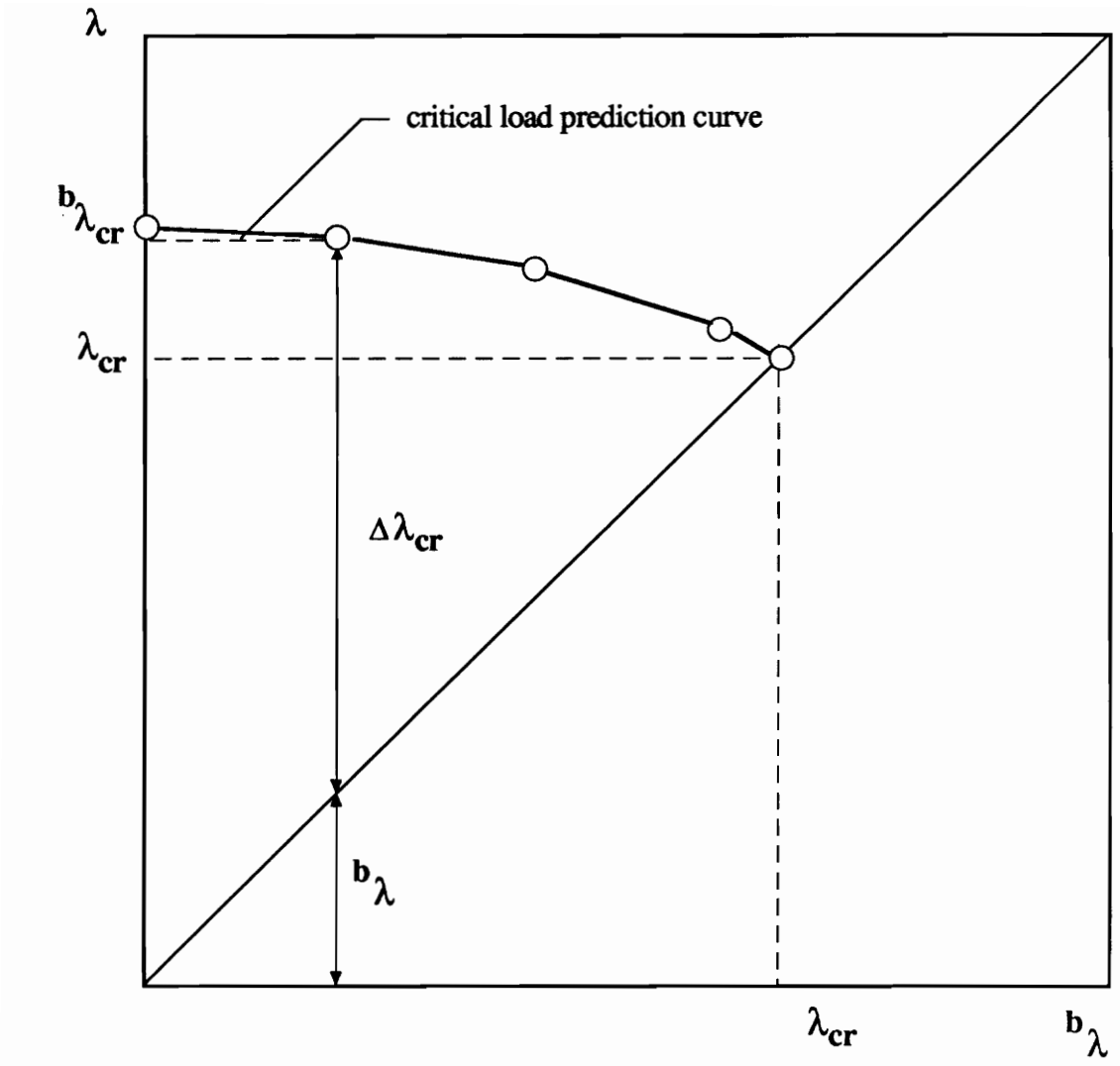

Fig. 5.1: Critical load parameters.

5.3.1 Uniform snow load

Table 5.1 shows the critical load factors corresponding to base load factors of 2, 3 and 4. The critical load factor obtained by nonlinear analysis was 4.45, which is very close to the results obtained here. It was not possible to get critical load factors for base load factors of 0 and 1, although different values of β were used. The critical load prediction curve (fig. 5.3) is almost a straight line, which indicates that the critical load can be obtained from as little as 2 points. The buckling mode can be obtained by plotting the deformed shape corresponding to the lowest eigenvalue. For this load case the buckling mode is similar to the one obtained by nonlinear analysis (twist buckling).

Table 5.1: Buckling load prediction for uniform snow load.

^{b}p (psf)	β	$^{b}\lambda$	p_j (psf)	C_{cr}	$^{b}\lambda_{cr}$	p_{cr} (psf)
15		0				
40		1				
60	0.05	2	1.25	50.01	4.50	127.5
80	0.05	3	1.25	29.33	4.47	126.7
100	0.05	4	1.25	9.20	4.46	126.5

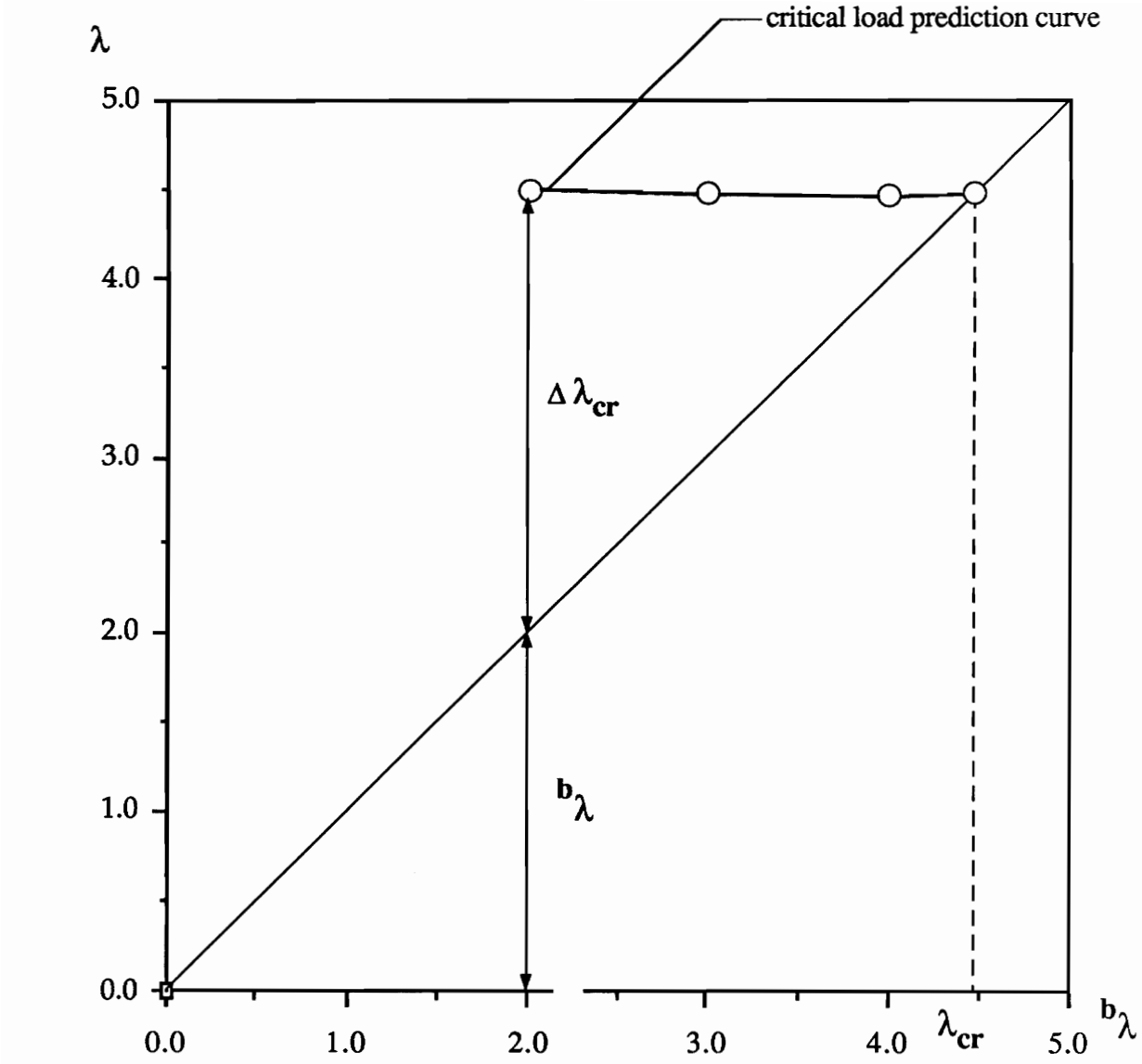

Fig. 5.2: Critical load prediction for uniform snow load.

5.3.2 Inner snow load

Critical load factors for base load factors of 0, 1, 2, 3 and 4 were obtained (Table 5.2). For small base load factors (0 and 1), very small values of β had to be used to get positive eigenvalues. The results are very close to that obtained from nonlinear analysis (λ_{cr}=4.62). The critical load prediction curve (fig. 5.3) is almost straight, which shows that the method is effective. A plot of the buckling mode corresponding to the lowest eigenvalue shows the same buckled shape obtained from nonlinear analysis (fig 4.4).

Table 5.2: Buckling load prediction for inner snow load.

b_p(psf)	β	p_j (psf)	$^b\lambda$	C_{cr}	$^b\lambda_{cr}$	p_{cr} (psf)
15	0.0001	0.0025	0	47634.0	4.76	119.0
40	0.001	0.025	1	3709.2	4.70	117.5
60	0.01	0.25	2	267.0	4.67	116.7
80	0.01	0.25	3	82.1	4.64	116.0
100	0.01	0.25	4	62.8	4.63	115.7

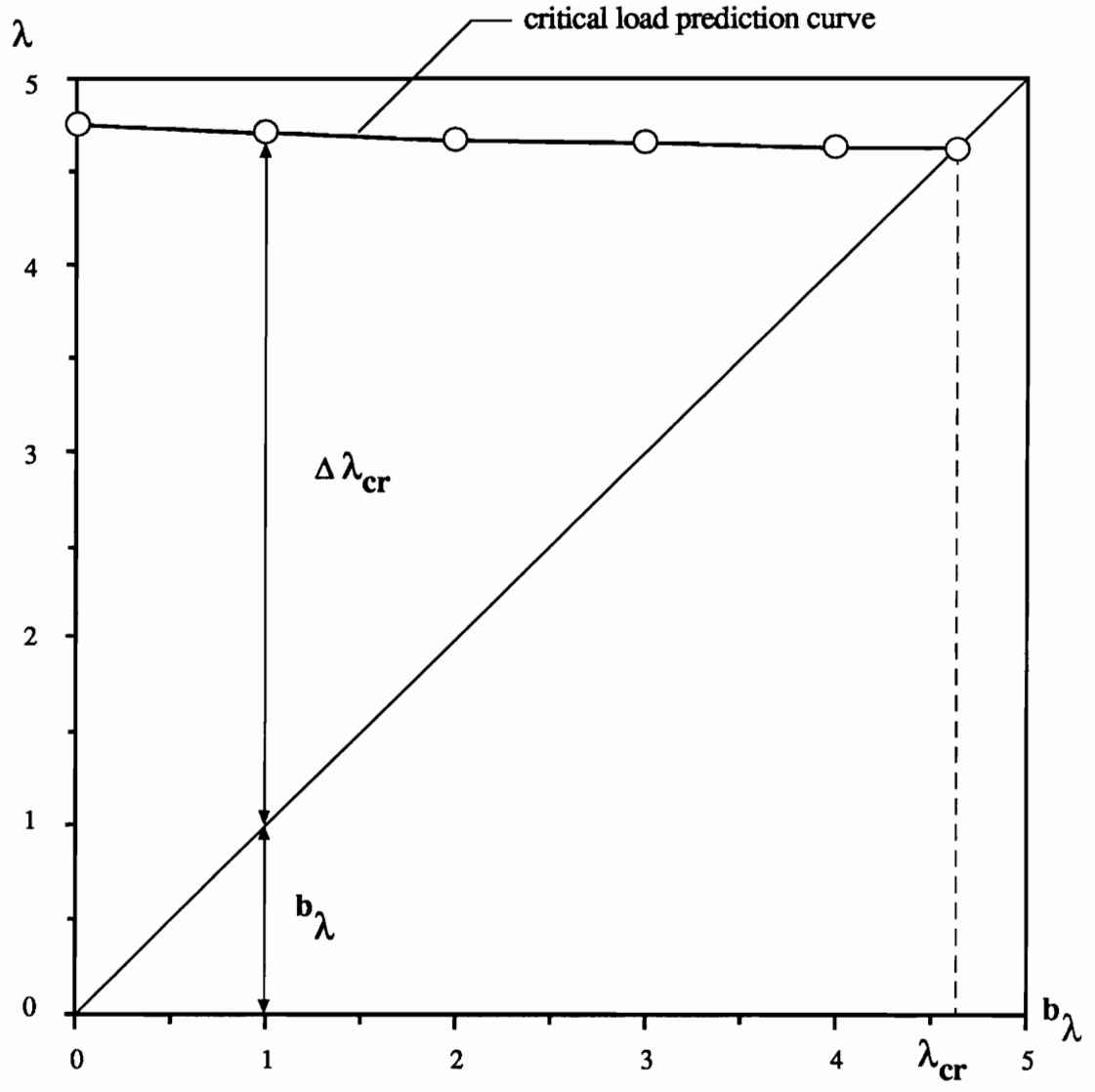

Fig. 5.3: Critical load prediction for inner snow load.

5.3.3 Outer snow load

The results for this load case were similar to those for uniform snow load. Critical load factors could not be obtained for base load factors of 0 and 1. This similarity in behavior is probably due to the similarity in buckling modes for uniform and outer snow loads. The critical load factors predicted are close to the one obtained from nonlinear analysis (Table 5.3). Figure 5.4 shows the critical load prediction curve, which is almost straight, proving the effectiveness of the method for this load case. As for the previous load cases, the buckling mode is identical to the one obtained from nonlinear analysis shown in fig 4.9.

Table 5.3: Buckling load prediction for outer snow load.

b_p(psf)	β	p_j (psf)	$^b\lambda$	C_{cr}	$^b\lambda_{cr}$	p_{cr}(psf)
15			0			
40			1			
60	0.001	0.025	2	3492.6	5.49	137.3
80	0.02	0.50	3	125.96	5.52	138.0
100	0.01	0.25	4	155.06	5.55	138.7

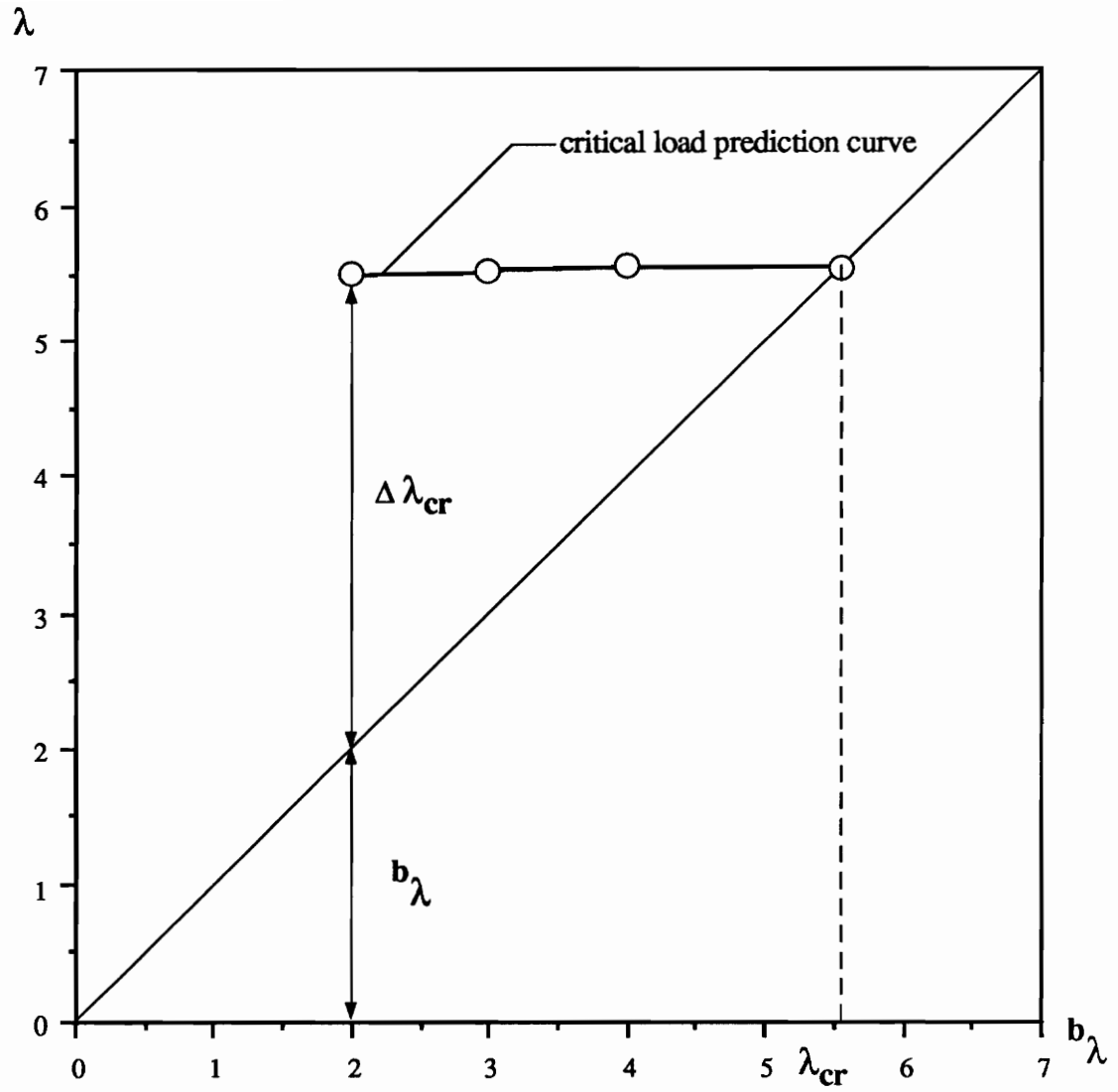

Fig. 5.4: Critical load prediction for outer snow load.

5.3.4 Snow over half the dome

The critical load factor obtained from nonlinear analysis was 6.0, which is far from the predicted values that ranged from 3.76 to 3.53 (Table 5.4). This discrepancy is shown in fig. 5.5. The critical load curve does not approach the critical load factor. Critical load factors for base load factors greater than 3 could not be obtained because the analysis resulted in negative eigenvalues. The buckling mode was identical to the one obtained by nonlinear analysis (fig. 4.12).

Table 5.4: Buckling load prediction for snow over half the dome.

b_p (psf)	β	p_j (psf)	λ_b	C_{cr}	${}^b\lambda_{cr}$	p_{cr} (psf)
15	0.0001	0.0025	0			
40	0.001	0.025	1	276.0	3.76	109.0
60	0.01	0.25	2	157.9	3.58	104.5
80	0.01	0.25	3	53.0	3.53	103.2
100	0.01	0.25	4			

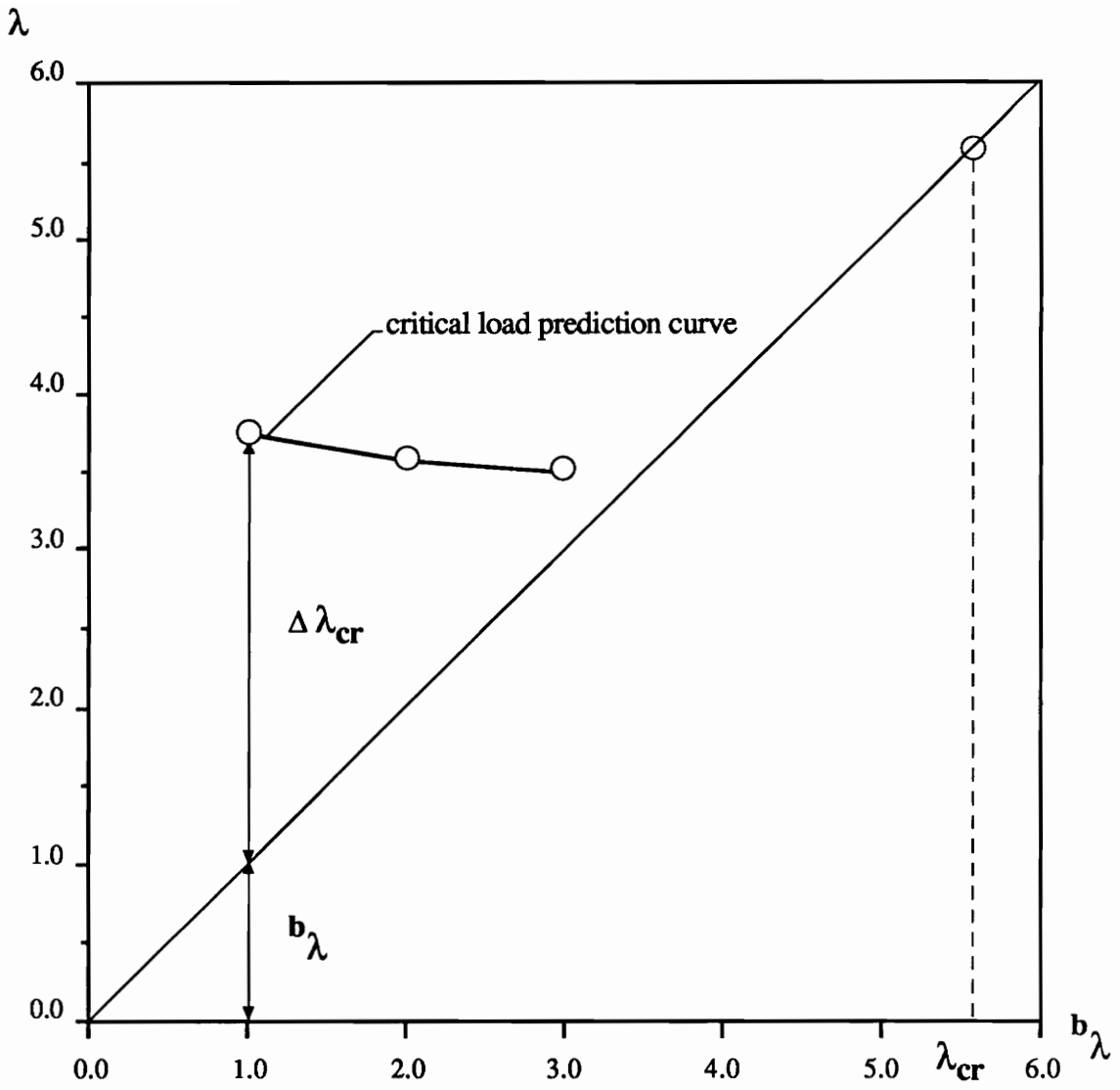

Fig. 5.5: Critical load prediction for snow over half the dome.

6. FLEXIBLE JOINTS

6.1 INTRODUCTION

Until now, all of the joints in the model were considered to be rigid, which does not reflect the real stiffness of the joints. A model for the joints with varying stiffness was needed to get a more realistic model. This part discusses the modeling of the joints and the underlying assumptions and limitations. Also, the effect of reducing the stiffness of the joints on the buckling load is investigated.

6.2 THE VARAX JOINTS

There are two types of connections to be considered:

1- Connections between the beams and the purlins

In the Varax dome the purlins are connected to the main beams via steel hangers. To simplify the analysis, the purlin connections are considered as pin joints and the purlins as truss elements. This simplification is consistent with the real behavior of the purlins, since they are intended to distribute the loads from the decking to the beams.

2- Connections between the main beams

The connections between the beams are made through patented steel hubs as shown in fig. 6.1. The hubs are very stiff in the axial direction; however, their bending stiffness is limited.

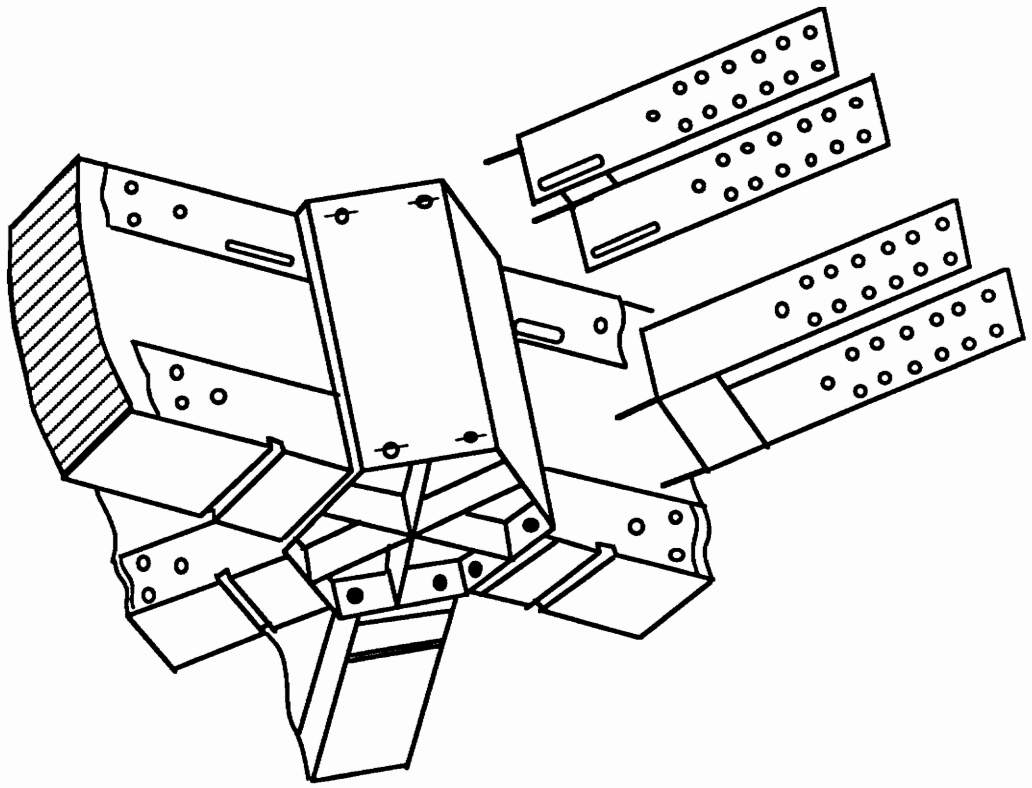

Fig. 6.1: The Varax joint.

6.3 ALTERNATIVES FOR MODELING THE JOINTS

Two alternatives were considered:

1- Using springs: The connections between the beams are modeled as springs. A spring element is placed between two nodes (6 in apart). This alternative was dismissed because it would be difficult to specify the orientations of the springs and the appropriate stiffness. Therefore, the method used by Davalos [3] in his research was used.

2- Using connector element:s Instead of springs, beam elements are used to model the connections, the connecting element is 6 in long and the cross sectional dimensions are varied to modify the moments of inertia and therefore the stiffness of the connection (fig 6.2).

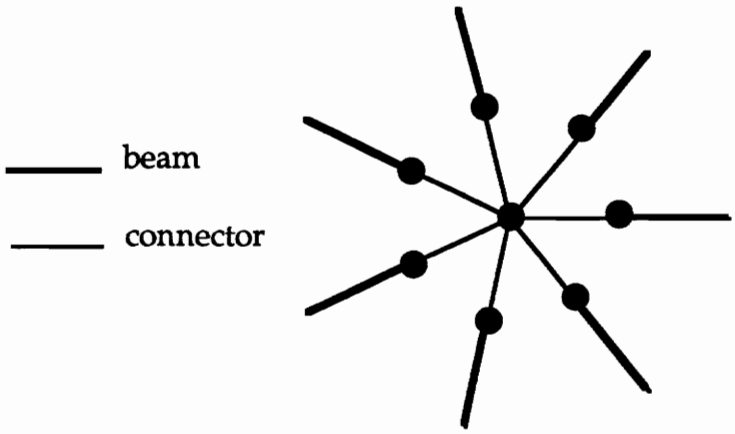

Fig. 6.2: Modeling of the beam connections (at apex).

6.4 STIFFNESS REDUCTION FACTOR

To determine the relation between the width and height reduction factor and the stiffness reduction factor, the moments of inertia of the original and reduced beams are related (fig 6.4). The goal is to find the width and height reduction factor, given a stiffness reduction factor. The relations for stiffness reduction factors of 75, 50 and 25% are presented in Table 6.1.

b: original width of beam
h: original height of beam
a: width and height reduction factor
c: stiffness reduction factor
I : original moment of inertia
I': connector moment of inertia

$$I = \frac{bh^3}{12}$$

$$I' = \frac{a^4 bh^3}{12}$$

$$I' = cI \Rightarrow c = a^4$$

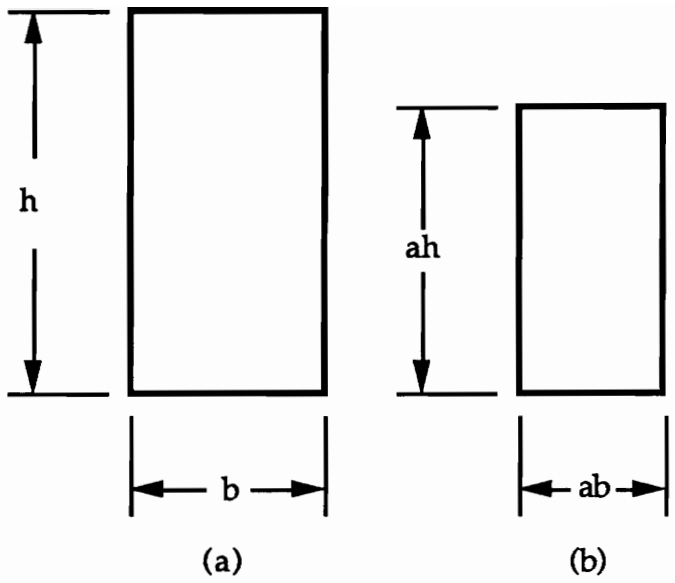

Fig. 6.3 (a) original beam dimensions; (b) connector beam element with reduced dimensions.

Table 6.1: Connector element dimensions for 3 stiffness reduction factors.

original height (in)	original width (in)	stiffness reduction factor (%)	width & height reduction factor (%)	reduced height (in)	reduced width (in)
12.0	5.125	25	29.3	8.5	3.6
		50	15.9	10.1	4.3
		75	6.9	11.2	4.8

6.5 MODELING THE JOINTS USING I-DEAS

To model the connections, nodes had to be created around the joints along the beams. To accomplish this, a useful node manipulation routine was used. First the node representing the joint is duplicated as many times as there are beams in the joint. Then, the orient command is used to translate each of the duplicate nodes along the beams.

The commands used are:

- Choose **orient** from the node menu.
- Choose **move along** from the orient menu.
- Select node.
- Select the two end nodes of the beam to define the vector to move along.
- Enter the distance to move.

Once the nodes are created, connector elements are defined. The modifications are done on one sector of the dome, which is then reflected to obtain the complete dome.

6.6 MODIFICATIONS TO THE DOME MODEL

The introduction of the connector elements increases both the number of nodes and the number of elements. Also, each purlin is modeled as a single truss element (instead of two beams). This necessitated the modification of the shell element pattern. Instead of using only triangular shell elements, quadrilateral shell elements had to be used to preserve symmetry of the shell

element mesh. This reduced the number of nodes that carry load from 274 to 218. Figure 6.4 shows the shell elements of the new model.

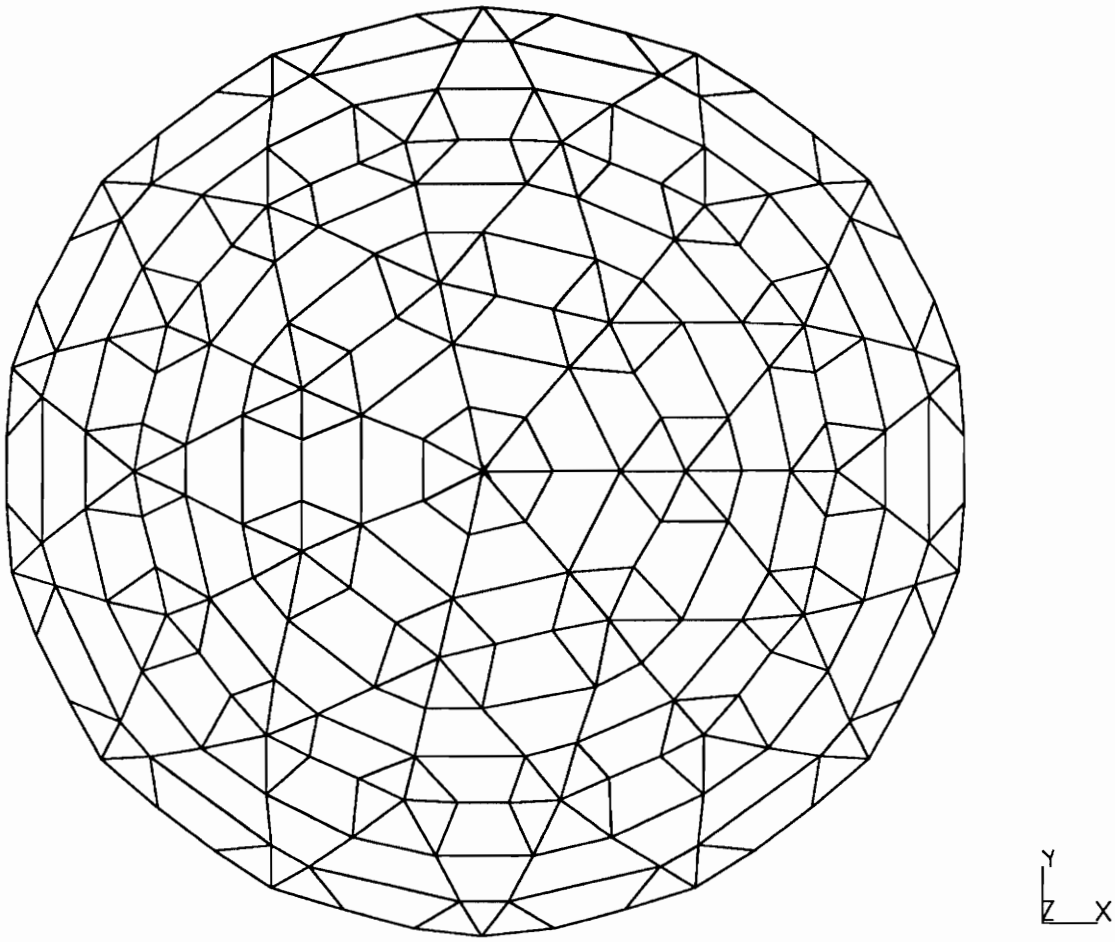

Fig. 6.4: Shell element mesh for flexible joint model.

6.7 RESULTS OF THE ANALYSES

Tables 6.2, 6.3, 6.4 and 6.5 show the results of nonlinear analyses for the four load cases investigated thus far for different joint stiffnesses. Modeling the purlins as truss elements and therefore making the connection between the purlins and the beams as pin connections had the most significant effect. The critical load factor was reduced by 55, 52, 51 and 30% for uniform, inner, outer and half snow loads respectively. This demonstrates the need for modeling the bracing to include its stiffening effect. The buckling modes obtained were identical to those obtained for the dome with rigid joints. Reducing the stiffness of the beam connections had a less drastic effect, especially for the symmetric load cases (uniform, inner and outer snow loads), with reductions in the critical load factors varying between 9 and 22%. For the snow over half the dome, the change was more significant: 38% reduction in the critical load factor for 75% reduction in the stiffness of the connections.

Table 6.2: Critical load factors for uniform snow load.

joint stiffness % of original stiffness	critical load factor	% change
rigid	2.0	———
50%	1.8	10
25%	1.6	20

Table 6.3: Critical load factors for inner snow load.

joint stiffness % of original stiffness	critical load factor	% change
rigid	2.2	———
50%	2.0	9
25%	1.8	18

Table 6.4: Critical load factors for outer snow load.

joint stiffness % of original stiffness	critical load factor	% change
rigid	2.7	———
50%	2.6	4
25%	2.3	15

Table 6.5: Critical load factors for snow over half the dome.

joint stiffness % of original stiffness	critical load factor	% change
rigid	4.2	———
50%		
25%	2.6	38

7. MODELING OF THE EFFECT OF THE DECKING

7.1 OVERVIEW

The dome is covered with 2 in tongue and groove decking which is nailed to the beams and purlins. The decking is parallel to the center line in each sector. In this part the method used to model the decking is introduced and the effect of the decking on the critical load for snow over the entire dome and snow over half the dome is investigated . The results are discussed and the validity of the method is assessed.

7.2 MODELING OF THE DECKING

The decking provides a certain amount of lateral support for the beams. Bracing consisting of steel truss elements is used to simulate the effect of the decking (fig. 7.1). The bracing elements have a cross sectional area of 0.5-in^2. The bracing consists of two patterns:

1• Cross bracing:	Intended to resist twist buckling of the dome (fig 7.2a).
1• Longitudinal bracing:	Intended to resist buckling of beams in the first and second ring about their weak axes (fig 7.2b).

Although these two types of bracing have different goals, they interact to provide resistance against both buckling modes associated with uniform snow load and snow over half the dome.

The truss elements are created using I-DEAS; then the element data are translated into the ABAQUS input file.

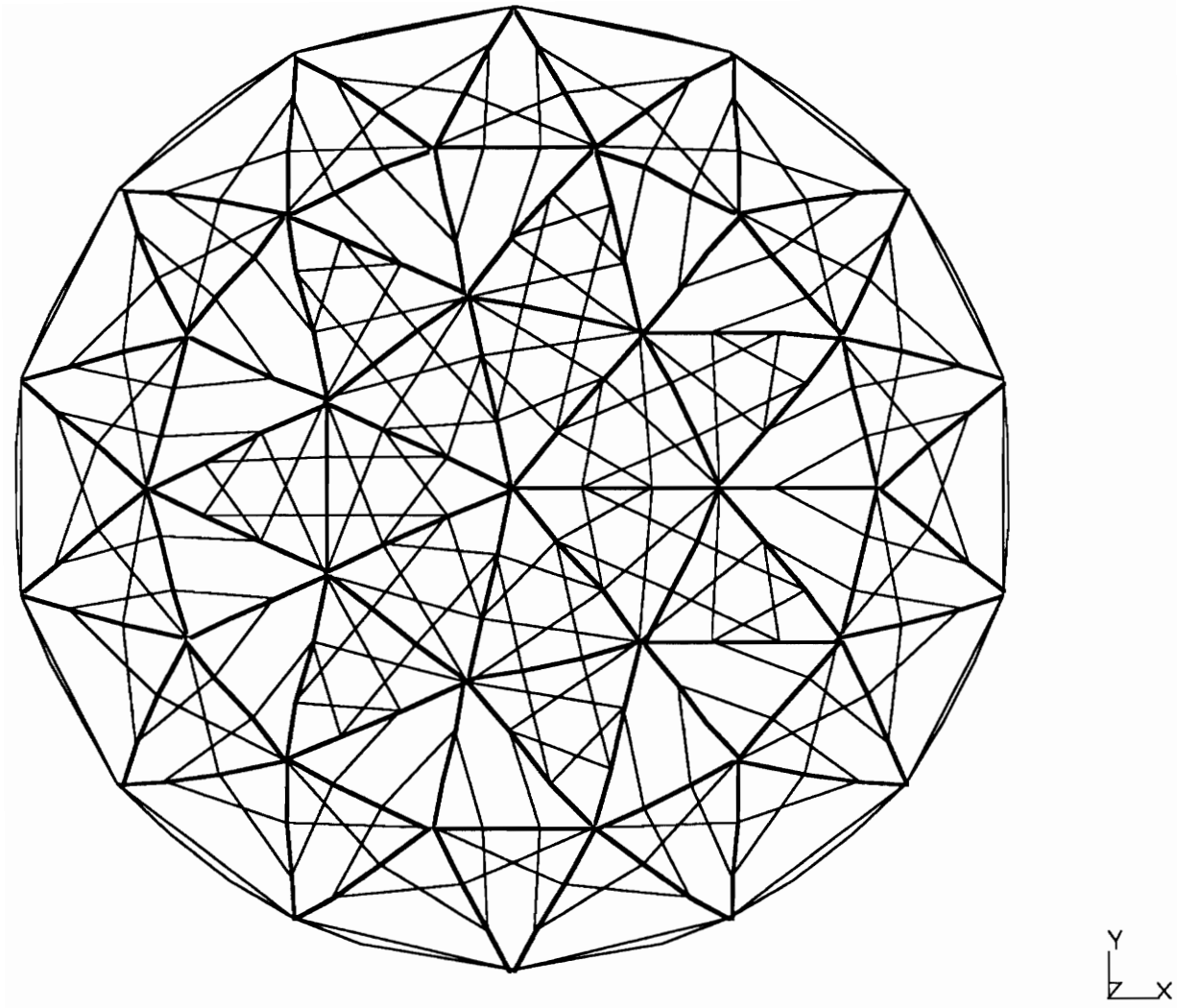

Fig. 7.1: Bracing for entire dome.

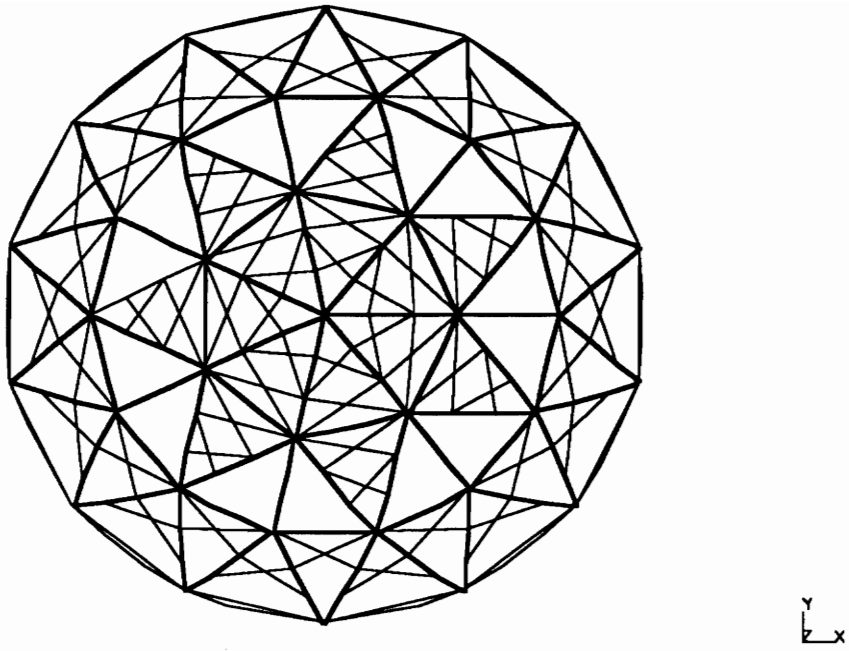

(a)

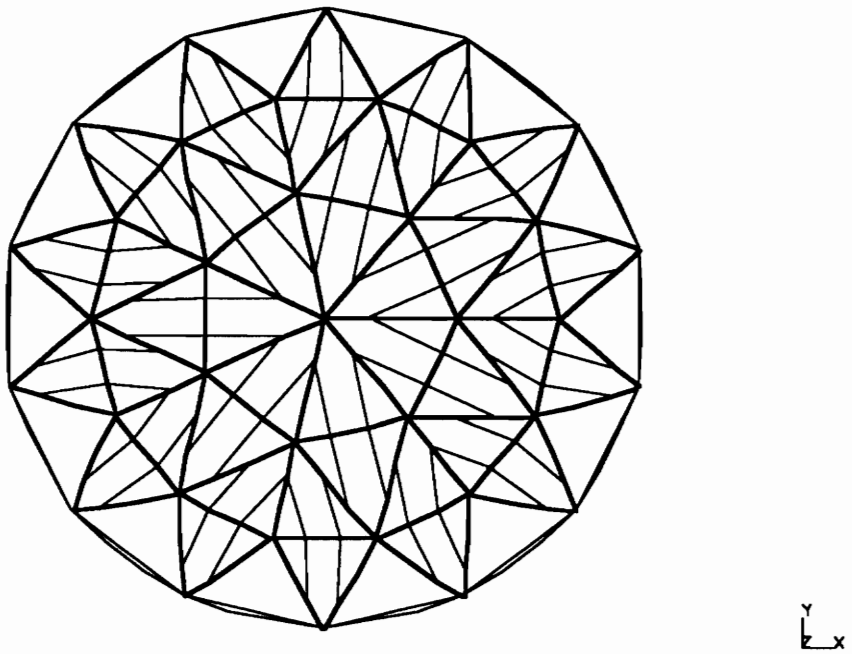

(b)

Fig. 7.2: Bracing on entire dome (a) cross bracing; (b) longitudinal bracing.

7.3 PROCEDURE

Combined linear and nonlinear critical load prediction was used to get an approximate value for the critical load factor. Then nonlinear analysis was used to get a more accurate critical load factor value for the two load cases considered. Stresses at some beams and at the bracing were monitored to check if they exceed the proportional limit and ultimate stresses.

7.4 RESULTS

7.4.1 Uniform snow load

The critical load factor was 11.8, which is six times the critical load factor without the bracing. However, at such high loads, the stresses in many beams exceed the ultimate compressive and tensile stresses. The stress in the bracing varied between 575 psi and 54,422 psi in tension (all the bracing was subjected to tensile stresses). The bracing effectively suppressed the twist buckling mode(fig 4.2). The buckled shape is shown in fig. 7.3.

7.4.2 Snow over half the dome

The critical load factor was 11.0, which is 2.6 times the value for the dome without bracing. As was the case for uniform snow, the stresses in many beams exceed the ultimate tensile and compressive stresses. Also, the stress in the bracing elements was very high: the values ranged from 83,000 psi in compression to 120,500 psi in tension. The buckled shape shown in fig. 7.4

demonstrates how the bracing suppressed the mode encountered for the dome without bracing (fig. 4.12).

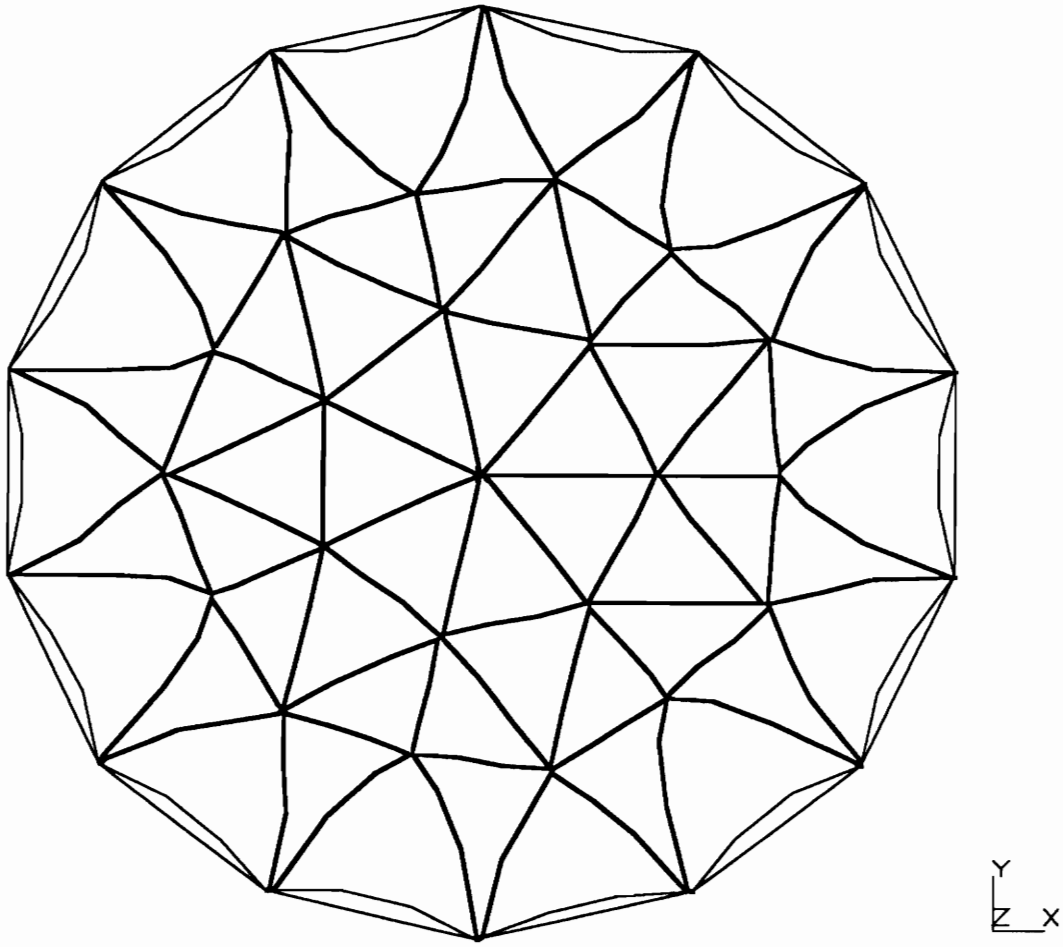

Fig. 7.3: Buckled shape for uniform snow load.

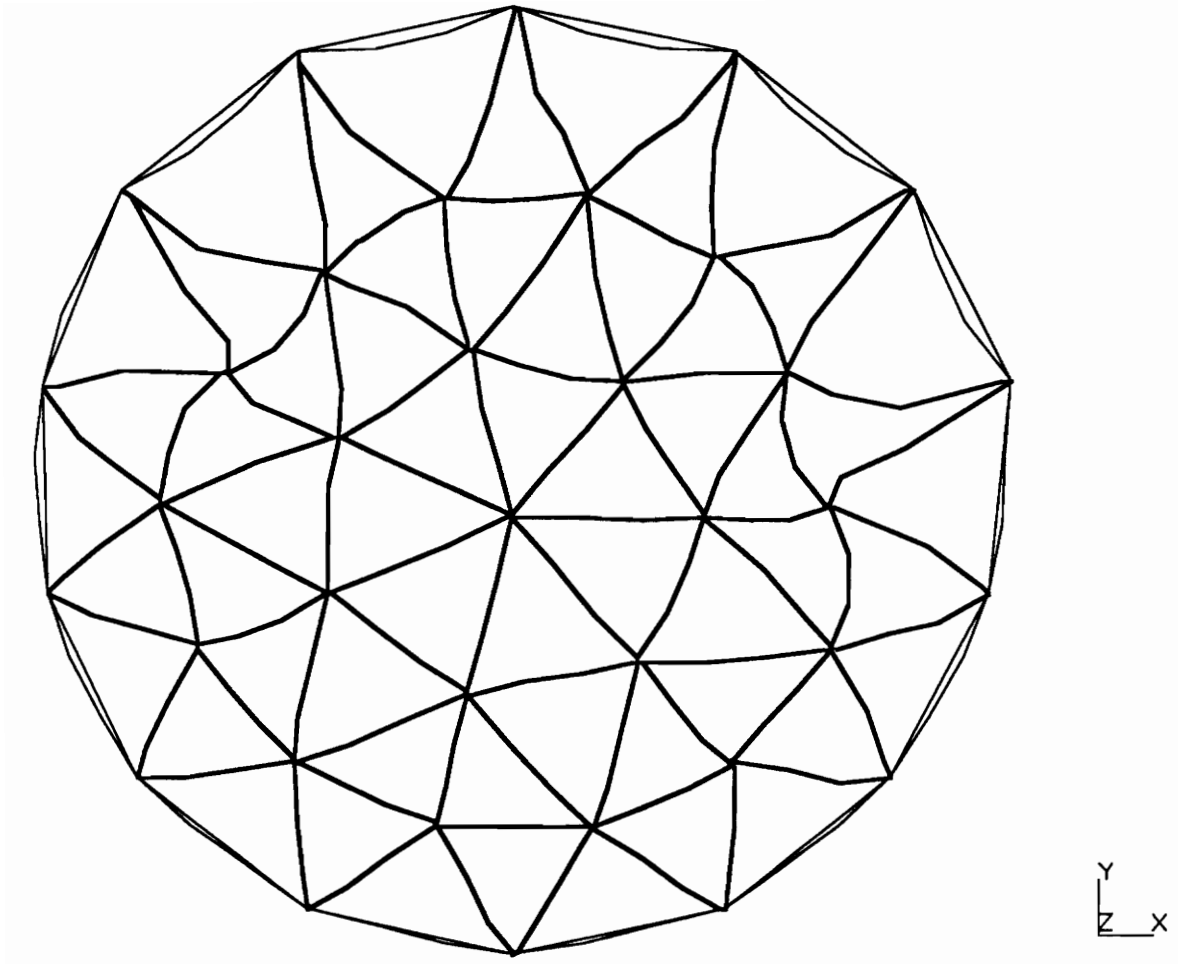

Fig. 7.4: Buckled shape for snow over half the dome.

7.5 DISCUSSION OF THE RESULTS

The bracing was effective in increasing the critical load factor by suppressing the buckling modes of the dome without bracing. However, the stresses in both the beams and the bracing were excessive. The bracing model should be modified such that the bracing elements carry only tensile forces. The strength of the decking needs to be investigated to obtain a better model for bracing.

8. CONCLUSIONS AND RECOMMENDATIONS

8.1 CONCLUSIONS

This study shows that depending on how the connections are modeled, two cases emerge:

1- Rigid connections

The critical load factor is relatively high, and the maximum stresses just before buckling are either close to the proportional limit (for the uniform, inner, and outer snow loads), or are beyond the ultimate point for case of the snow over half the dome.

2- Flexible connections

Modeling the connections between the purlins and the beams as pin connections drastically reduces the critical load factor (as much as 50%). Reducing the stiffness of the connections between the beams further reduces the critical load.

Changing the flexibility of the connections does not change the buckling modes for each load case; it only reduces the critical load by a factor of 9 to 22% for the symmetric load cases and 38% for snow over half the dome.

It was also shown that the critical load can be increased by strategically applying truss bracing to simulate the action of the decking, which was ignored thus far. However, this leads to stresses beyond the ultimate point.

The combined linear and nonlinear buckling prediction proved to be a valuable tool for predicting both critical loads and buckling modes. However, the critical load predicted for snow over half the dome was 20% below the critical load obtained from nonlinear analysis for $^{b}\lambda$ equal to three.

8.2 RECOMMENDATIONS

Because the material does not remain elastic (when decking is considered), it is necessary to include material nonlinearities in future nonlinear analyses. This will require experimental research into the behavior of timber beyond the proportional limit to obtain nonlinear material laws.

By predicting the possible buckling modes of domes, it is possible to design appropriate safeguards against instability.

REFERENCES

1. ABAQUS, General-Purpose Finte Element System, Hibbit, Karlson & Sorensen, Inc., 100 Medway Street, Providence, RI.

2. Bathe, K. J., Finite Element Procedures in Engineering Analysis, Prentice-Hall, Englewood Cliffs, NJ, 1982.

3. Davalos, J. F., Geometrically Nonlinear Finite Element Analysis of a Glulam Timber Dome, Ph. D. Dissertation, Virginia Polytechnic Institute and State University, July, 1989.

4. Davalos, J. F., Loferski, J. R., and Holzer, S. M.,"Modeling of Glued-Laminated Timber Beams as Transversely Isotropic," Journal of Materials, ASCE, to appear.

5. Holzer, S. M., Davalos, J. F., and Huang, C. Y., "A Review of Finite Element Stability Investigations of Spatial Wood Structures," Bulletin of the International Association for Shell and Spatial Structures, to appear.

6. Holzer, S. M., Wu, C. H., and Tissaoui, J., "Finite Element Stability Analysis of a Glulam Dome," International Journal of Space Structures, to appear.

7. Huang, C. Y., Geometrically Nonlinear Finite Element Analysis of a Lattice Dome, M.S. Thesis, Virginia Polytechnic Institute and State University, January 1990.

8. I-DEAS, Engineering Analysis, Model Solution and Optimization, MacNeal-Schwendler, Structural Dynamics Research Corporation, 2000 Eastman Drive, Milford, Ohio.

9. Ramm, E., and Stegmuller, H., "The Displacement Finite Element Method in Nonlinear Buckling Analysis of Shells," Proceedings of a State-of-the-Art Colloquium in Buckling of Shells, Universitat Stuttgart, Germany, 1982, pp. 201-235.

10. Zienkiewicz, O. C., The Finite Element Method in Engineering Science, McGraw-Hill, London, 1971.

APPENDIX A

```
C=====================================================================
C   PROGRAM TO DETERMINE THE DIRECTION COSINES OF THE BEAMS AND      C
C   PURLINS OF THE CHURCH OF THE NAZARENE VARAX DOME                 C
C   VARIABLES:                                                       C
C   N:          NODE NUMBER                                          C
C   NE:         ELELEMNT NUMBER                                      C
C   X, Y, Z:    NODE COORDINATES                                     C
C   R:          RADIUS OF THE DOME                                   C
C   XCOS, YCOS, ZCOS:   COORDINATES OF 1 AXIS VECTOR FOR THE BEAM    C
C   XNORM:   MAGNITUDE OF 1 AXIS VECTOR                              C
C   XCC, YCC, ZCC:   DIRECTION COSINES FOR THE BEAM                  C
C=====================================================================
C
C       DECLARE THE VARIABLES
C
   REAL        X, Y, Z
   REAL        XCOS(715), YCOS(715), ZCOS(715)
   REAL        XC(715), YC(715), ZC(715)
   REAL        XCC(715),YCC(715), ZCC(715)
   REAL        R = 1272.0
   INTEGER     I, N, NE, N1, N2
C
C       OPEN NODE COORDINATES AND ELEMENT CONNECTIVITY DATA FILES
C
    OPEN(UNIT=55,STATUS='OLD')
    OPEN(UNIT=60,STATUS='OLD')
    OPEN(UNIT=65,STATUS='OLD')
    OPEN(UNIT=70,STATUS='OLD')
    OPEN(UNIT=75,STATUS='OLD')
C
C       OPEN OUTPUT FILES
C
    OPEN(UNIT=88,STATUS='UNKNOWN')
    OPEN(UNIT=98,STATUS='UNKNOWN')
CC      READ NODES AND THEIR COORDINATES
   DO 10 I=1,442
     READ (55,*) N, X, Y, Z
     XCOS(I) = X
     YCOS(I) = Y
     ZCOS(I) = Z
10   CONTINUE
CC      READ  BEAM CONNECTIVITY DATA AND COMPUTE DIRECTION COSINES
   DO 20 I=1,231
     READ (60,*) NE, N1, N2
      XC(NE) =   YCOS(N1) * ZCOS(N2) - ZCOS(N1) * YCOS(N2)
      YC(NE) = -(XCOS(N1) * ZCOS(N2) - ZCOS(N1) * XCOS(N2))
```

```
      ZC(NE) =   XCOS(N1) * YCOS(N2) - YCOS(N1) * XCOS(N2)
       XNORM = (XC(NE)**2+YC(NE)**2+ZC(NE)**2) ** 0.5
      XCC(NE) = XC(NE) / XNORM
      YCC(NE) = YC(NE) / XNORM
      ZCC(NE) = ZC(NE) / XNORM
CC       WRITE ABAQUS ELEMENT DATA CARDS
      WRITE (88,200) NE
      WRITE (88,220) NE, N1, N2
      WRITE (98,230) NE
      WRITE (98,240)
       WRITE (98,250) XCC(NE),YCC(NE),ZCC(NE)
20   CONTINUE
CC       READ  SHORT PURLIN CONNECTIVITY DATA AND COMPUTE DIRECTION
CC       COSINES
    DO 30 I=1,56
      READ (65,*) NE, N1, N2
       XC(NE) = YCOS(N1) * ZCOS(N2) - ZCOS(N1) * YCOS(N2)
       YC(NE) = -(XCOS(N1) * ZCOS(N2) - ZCOS(N1) * XCOS(N2))
       ZC(NE) = XCOS(N1) * YCOS(N2) - YCOS(N1) * XCOS(N2)
       XNORM = (XC(NE)**2+YC(NE)**2+ZC(NE)**2) ** 0.5
      XCC(NE) = XC(NE) / XNORM
      YCC(NE) = YC(NE) / XNORM
      ZCC(NE) = ZC(NE) / XNORM
CC       WRITE ABAQUS ELEMENT DATA CARDS
      WRITE (88,200) NE
      WRITE (88,220) NE, N1, N2
      WRITE (98,230) NE
      WRITE (98,340)
       WRITE (98,250) XCC(NE),YCC(NE),ZCC(NE)
30   CONTINUE
CC       READ  LONG PURLIN CONNECTIVITY DATA AND COMPUTE DIRECTION
CC       COSINES
    DO 40 I=1,112
      READ (70,*) NE, N1, N2
       XC(NE) = YCOS(N1) * ZCOS(N2) - ZCOS(N1) * YCOS(N2)
       YC(NE) = -(XCOS(N1) * ZCOS(N2) - ZCOS(N1) * XCOS(N2))
       ZC(NE) = XCOS(N1) * YCOS(N2) - YCOS(N1) * XCOS(N2)
       XNORM = (XC(NE)**2+YC(NE)**2+ZC(NE)**2) ** 0.5
      XCC(NE) = XC(NE) / XNORM
      YCC(NE) = YC(NE) / XNORM
      ZCC(NE) = ZC(NE) / XNORM
CC       WRITE ABAQUS ELEMENT DATA CARDS
      WRITE (88,200) NE
      WRITE (88,220) NE, N1, N2
      WRITE (98,230) NE
      WRITE (98,440)
       WRITE (98,250) XCC(NE),YCC(NE),ZCC(NE)
40   CONTINUE
CC       READ  EDGE PURLIN CONNECTIVITY DATA AND COMPUTE DIRECTION
CC       COSINES
    DO 60 I=1,42
```

```
      READ (75,*) NE, N1, N2
       XC(NE) = YCOS(N1) * ZCOS(N2) - ZCOS(N1) * YCOS(N2)
       YC(NE) = -(XCOS(N1) * ZCOS(N2) - ZCOS(N1) * XCOS(N2))
       ZC(NE) = XCOS(N1) * YCOS(N2) - YCOS(N1) * XCOS(N2)
        XNORM = (XC(NE)**2+YC(NE)**2+ZC(NE)**2) ** 0.5
      XCC(NE) = XC(NE) / XNORM
      YCC(NE) = YC(NE) / XNORM
      ZCC(NE) = ZC(NE) / XNORM
CC       WRITE ABAQUS ELEMENT DATA CARDS
      WRITE (88,200) NE
      WRITE (88,220) NE, N1, N2
      WRITE (98,230) NE
      WRITE (98,540)
       WRITE (98,250) XCC(NE),YCC(NE),ZCC(NE)
60   CONTINUE
CC       FORMAT STATEMENTS
200   FORMAT (T1,'*ELEMENT,TYPE=B33,ELSET=E',T26,I3)
220    FORMAT (1X,I4,',',I4,',',I4)
230   FORMAT (T1,'*BEAM SECTION,SECTION=RECT,MATERIAL=WOOD,ELSET=E',T49,
  $      I3)
240   FORMAT (2X,'5.125,12.0')
250    FORMAT (1X,F9.4,',',F9.4,',',F9.4)
340   FORMAT (2X,'3.125,7.5')
440   FORMAT (2X,'5.125,7.5')
540   FORMAT (2X,'3.125,22.0')
      END
```

VITA

Jacem Tissaoui was born in Jendouba a small town in the north-west of Tunisia in December of 1967. He received his Bachelor of science in Civil Engineering from Pennsylvania State University in 1989. He was then accepted in the graduate program in the Civil Engineering department at Virginia Polytechnic Institute and State University where he is pursuing his studies towards a Ph. D. degree.